Research article

JHEP|Reports

Macrophage Notch1 signaling modulates regulatory T cells via the TGFB axis in early MASLD

Mengya Zhang[1,†], **Kun Li**[2,†], Xiaoxing Huang[4], Dongqin Xu[1], Ruobin Zong[3], Qintong Hu[1], Xiaoyu Dong[1], Qinyong Zhang[1], Chaochen Jiang[1], Yue Ge[1], Changyong Li[3,*], Jie Ping[1,*]

JHEP Reports **2025**. vol. 7 | 1–14

Background & Aims: Hepatic immune imbalance is crucial for driving metabolic dysfunction-associated steatotic liver disease (MASLD) progression. However, the role of hepatic regulatory T cells (Tregs) in MASLD initiation and the mechanisms responsible for their change are not completely understood.

Methods: A mouse model subjected to a short-term high-fat diet (HFD) to mimic early steatosis, along with liver biopsy samples from patients with simple steatosis, and macrophage-specific Notch1-knockout mice (Notch1$^{M\text{-}KO}$), were used to investigate the role of Tregs in early MASLD and the effect of hepatic macrophage Notch1 signaling on Treg frequency. The miRNAs correlated with Treg differentiation were analyzed using exosomal miRNA sequencing.

Results: A decrease in Tregs contributed to HFD-induced hepatic steatosis and insulin resistance (five/group/time point, p <0.001). Remarkably, the frequency of Tregs was negatively correlated with Notch1 activation in hepatic macrophages during hepatic steatosis (38/group, r = -0.735, p <0.001). Furthermore, Notch1 deficiency attenuated hepatic lipid deposition and reversed Treg levels (five/group, p <0.01 and <0.05, respectively). Moreover, Treg depletion in Notch1$^{M\text{-}KO}$ mice greatly diminished the ameliorative effect of macrophagic Notch1 deletion on hepatic steatosis. Mechanistically, macrophage Notch1 activation increased the level of exosomal miR-142a-3p (by one- to two- fold), impairing Treg differentiation by targeting transforming growth factor beta receptor 1 (TGFBR1) on T cells. Consistently, HFD-fed Notch1$^{M\text{-}KO}$ mice exhibited reduced miR-142a-3p levels, elevated TGFBR1 expression on T cells, and increased Treg frequency in the liver.

Conclusions: These findings highlight the crucial role of hepatic Tregs during the early stage of MASLD and add a novel, non-negligible pathway for macrophage involvement in hepatic steatosis. We identify a previously unrecognized molecular mechanism involving the macrophage Notch1/exosomal miR-142a-3p/TGFBR1 pathway in regulating Treg differentiation, providing a rationale for refined therapeutic strategies for MASLD.

Introduction

Metabolic dysfunction-associated steatotic liver disease (MASLD), formerly known as nonalcoholic fatty liver disease, initiating from simple steatosis to steatohepatitis (metabolic dysfunction-associated steatohepatitis; MASH), ultimately leading to fibrosis, and hepatocellular carcinoma, has emerged as the leading cause of gastrointestinal diseases, affecting ~25% of the population worldwide.[1] Nevertheless, there are currently no FDA-approved pharmacological therapies for MASLD, given that the molecular mechanisms involved have not been fully elucidated, highlighting the need for deeper insights into the mechanisms underlying MASLD and the identification of novel therapeutic strategies.

Several hypotheses have been proposed regarding the pathogenesis of MASLD, from '2-hit' to 'multi-hit', which involve lipotoxicity, oxidative stress, mitochondrial injury, immune imbalance, and inflammatory cytokine production.[2] Among these factors, immune imbalance is a crucial element in driving MASLD progression.[3] While pronounced inflammation may only be observed during MASH, profound alterations of the hepatic immune system occurring even during steatosis, indicating the involvement of the immune system across the entire MASLD spectrum.[4] Regulatory T cells (Tregs), a distinct lineage of CD4$^+$ T lymphocytes, have a crucial role in peripheral immune tolerance, especially in the liver.[5] The fine-tuning of Tregs is thought to contribute to the development of various liver diseases.[6,7] Previous studies found that the frequency of hepatic Tregs is reduced during MASH,[8] but increased during its premalignant stage.[9] These findings suggested the Tregs undergo dynamic changes during MASLD progression. Recently, adipose Tregs were shown to directly modulate lipid metabolism.[10] Hepatic steatosis is generally considered to be a

* Corresponding authors. Address: Wuhan University TaiKang Medical School (School of Basic Medical Sciences), 185 East Lake Road, Wuhan 430071, China. Tel.: +86 27 6875 9310.
E-mail addresses: pingjie@whu.edu.cn (J. Ping), lichangyong@whu.edu.cn (C. Li).
† Authors share co-first authorship.
https://doi.org/10.1016/j.jhepr.2024.101242

key initiating event in MASLD;[11] however, the role of hepatic Tregs in hepatic steatosis is not completely clear.

The liver is a vital place for peripherally induced Tregs because it has unique tolerogenic properties that favor the differentiation of antigen-specific Tregs.[12] The production of hepatic Tregs depends on multiple cells, including macrophages.[12] In particular, given the high plasticity of macrophages, different macrophage phenotypes exert diverse effects on Treg differentiation. Under homeostatic conditions, macrophages can induce $CD4^+$ T cells to differentiate into Tregs to maintain hepatic immune tolerance. However, this differentiation is impaired when macrophages display a proinflammatory phenotype.[13] Of note, previous studies demonstrated that hepatic macrophages preferentially polarize into a proinflammatory phenotype and recruit more proinflammatory cells into the liver during the initiation and development of MASLD.[14,15] Nevertheless, whether and how macrophages regulate Tregs in initiating MASLD remain elusive.

Exosomes (Exos), which have emerged as crucial mediators of intercellular communication, carry and deliver miRNAs, proteins, and metabolites from host cells to recipient cells.[16] Their contents are tightly regulated by physiological and pathological stimuli and highly dependent on the cell type.[17] Remarkably, Notch1 signaling has been reported to regulate miRNA expression and Exo release.[18,19] In addition, emerging reports indicate that Notch signaling has a crucial role in both innate and adaptive immunity,[20,21] and the Notch1 activation-mediated proinflammatory transforming effect of macrophages is involved in multiple chronic inflammatory diseases.[22,23] Thus, Notch1 signaling could be a potential modulating machinery for the crosstalk between macrophages and Tregs.

In the present study, we revealed the crucial role of hepatic Tregs and their correlation with Notch1 activation in hepatic macrophages during the early stages of MASLD. Using macrophage-specific Notch1-knockout ($Notch1^{M\text{-}KO}$) mice, we identified that macrophage-derived Exo-miR-142a-3p regulated by Notch1 impedes Treg production during hepatic steatosis. Our findings provide novel molecular insights into macrophage–Treg interactions, targeting of which might offer a potential strategy for preventing MASLD.

Materials and methods

Animals

Floxed Notch1 ($Notch1^{FL/FL}$) mice (Jackson Laboratory, Bar Harbor, ME, USA) and Lyz2-Cre mice (LysM-Cre; Jackson Laboratory) were used to generate $Notch1^{M\text{-}KO}$ mice. Mouse genotyping was performed by PCR of the tail DNA (Fig. S1). Male $Notch1^{FL/FL}$ and $Notch1^{M\text{-}KO}$ mice aged 8 weeks were used in the experiments.

Methodological details are provided in the Supplementary information online.

Isolation of Exos

Exo purification was achieved through differential ultracentrifugation. Briefly, the supernatant was collected after culturing bone marrow-derived macrophages (BMDMs) in Exo-free medium for 48 h. Exos were isolated via five sequential centrifugation steps at 4 °C: (1) 10 min at 300 × *g* to remove cells; (2) 10 min at 2,000 × *g* to remove cell debris; (3) 30 min at 10,000 × *g* to break organelles; (4) ultracentrifugation at 100,000 × *g* for 120 min to pellet exosomes; and (5) washing with a large amount of ice-cold PBS and ultracentrifuge at 100,000 *g* for 120 min. Exos were then resuspended in PBS and stored at −80 °C until use.

miRNA sequencing and data analysis

miRNA sequencing was done on RNA from BMDMs-Exos by Novogene (Beijing, China). Briefly, 2 μg of total RNA was used to prepare the miRNA library after checking the RNA quality and integrity. Then, miRNA sequencing was performed on TruSeq SR Cluster Kit v3-cBot-HS (Illumina) following the manufacturer's instructions. Differential expression analysis of the 2 groups was performed using the DESeq R package (version 1.24.0; R Foundation for Statistical Computing, Vienna, Austria). Sequencing data have been deposited in the SRA database (www.ncbi.nlm.nih.gov/sra) with the following accession number: PRJNA1046700.

Details of other methods are described in the Supplementary information online.

Results

Reduction in hepatic Tregs contributes to HFD-induced hepatic steatosis and insulin resistance

To evaluate the changes in Tregs during the initiation of MASLD, we analyzed the proportion and number of hepatic $CD4^+CD25^+Foxp3^+$ Tregs and the mRNA level of *foxp3,* a specific marker of Tregs, in liver tissues from HFD-fed mice at 1, 2, 4, and 6 weeks after the start of HFD feeding. Compared with the normal chow diet (NCD) group, the decline in hepatic $CD4^+CD25^+Foxp3^+$ Tregs was obvious, starting at 1 week and continuing until 6 weeks of HFD feeding, as determined by flow cytometry and quantitative reverse transcription (RT-qPCR) (Fig. 1A–C). As expected, multiple indices of HFD mice, including body weight, serum lipid levels, and intrahepatic lipid content, were higher than those of the NCD group (Fig. S2). Consistent with the murine model, fewer Tregs were observed in the steatotic human liver compared with the control group (Fig. 1D).

Next, to further clarify whether hepatic steatosis was directly correlated with the reduced Treg frequency, we constructed Treg-depleted mice and Treg-expanded mice by intraperitoneal injection of anti-CD25 antibodies[24] and low-dose IL-2 (ldIL-2),[25] respectively. There was a remarkable reduction in hepatic Tregs after anti-CD25 antibody administration, whereas ldIL-2 administration resulted in a significant increase in hepatic Tregs (Fig. 1E). After 4 weeks of HFD feeding, Treg-depleted mice showed higher body weight gain, whereas Treg-expanded mice showed lower body weight gain, although the difference was not significant (Fig. 1F). Glucose and insulin tolerance testing (GTT and ITT, respectively) showed that Treg-depleted mice had lower glucose tolerance and insulin sensitivity compared with HFD mice, whereas these phenomena were improved in Treg-expanded mice (Fig. 1G). Consistent with the systemic insulin resistance (IR), insulin signaling, as measured by the phosphorylation of Akt at S473 (pAkt), was impaired in the liver of Treg-depleted mice, but promoted in Treg-expanded mice (Fig. 1H). In addition, total cholesterol (TC)

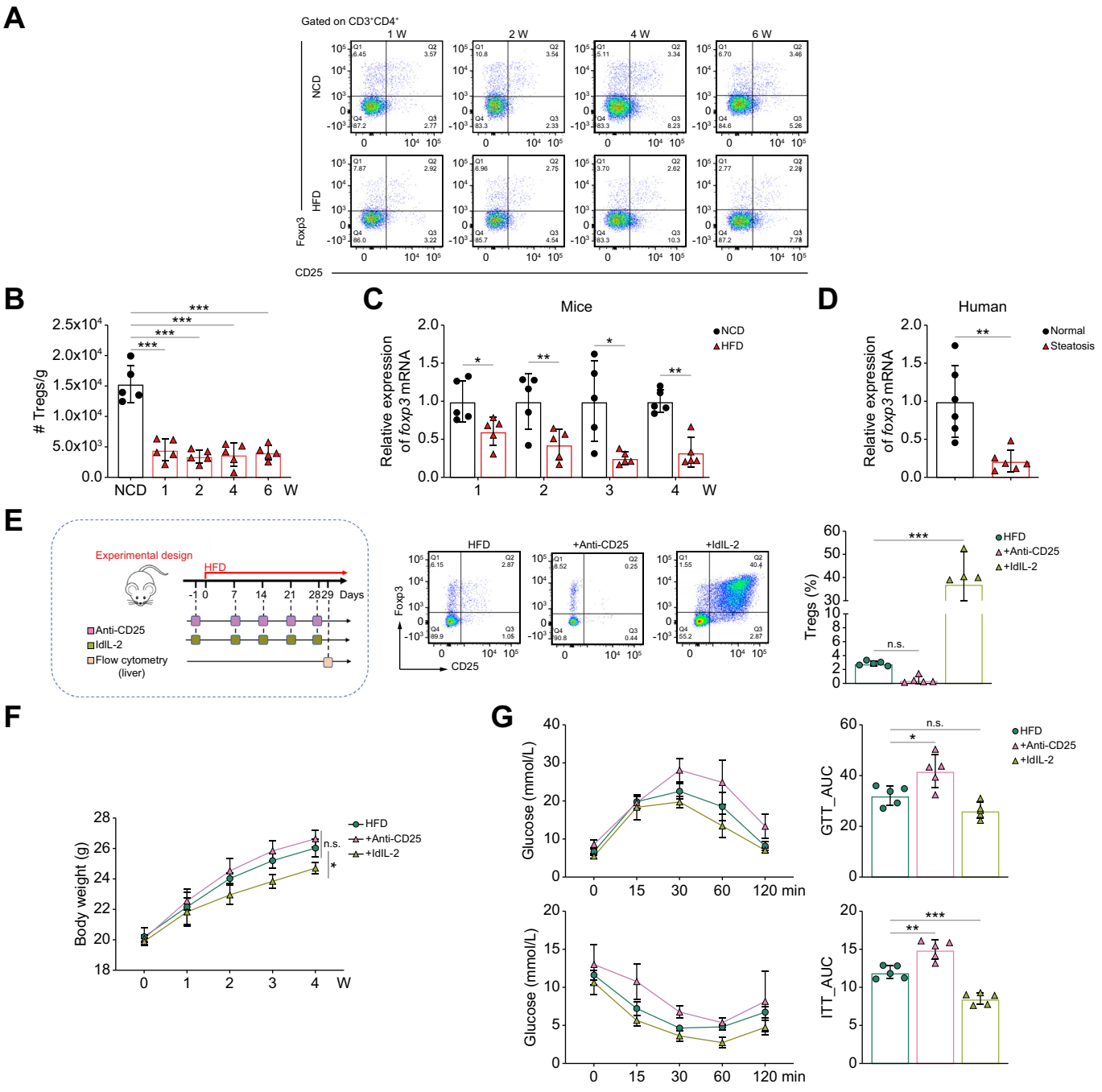

Fig. 1. Frequency of Tregs is associated with HFD-induced hepatic steatosis and insulin resistance. (A) Representative flow plots of the proportion of hepatic CD25$^+$Foxp3$^+$ Tregs gated on CD3$^+$CD4$^+$ T cells from mice fed a NCD or HFD (—four to five/group). (B) Number of hepatic CD4$^+$CD25$^+$Foxp3$^+$ Tregs of mice fed a NCD or HFD for 1, 2, 4, and 6 weeks (five/group). (C, D) *Foxp3* mRNA expression of liver tissues from (C) the NCD or HFD group (five/group), and (D) patients with or without hepatic steatosis (six/group). (E) Schematic of the construction of Treg-depleted mice (injected intraperitoneally with anti-CD25 antibodies) and Treg-expand mice (injected intraperitoneally with IdIL-2): representative dot plots of CD25$^+$Foxp3$^+$ Tregs gated on CD3$^+$CD4$^+$ T cells in the liver and a graph of the proportion of hepatic CD4$^+$CD25$^+$Foxp3$^+$ Tregs (five/group). Comparison of (F) body weight (five/group), (G) GTT and ITT (five/group), (H) insulin-stimulated Akt and pAkt expression in the liver (three/group), (I) serum TC and total TG levels (five/group), and liver TC and TG levels (five/group) in Treg-depleted *vs.* Treg-expanded mice. (J) Representative images of H&E and Oil red O staining of liver sections (scale bars: 50 μm and 100 μm, respectively). (K) Representative images of Oil red O staining (scale bar: 100 μm) and TG content of primary hepatocytes co-cultured with Tregs or not (three/group). (L) Immunoblot analysis of insulin-stimulated Akt and pAkt in primary hepatocytes co-cultured with Tregs or not (three/group). Values represent means ± SD. Statistical analysis was performed by 2-tailed unpaired Student *t* test (B–D) or one-way ANOVA and Tukey's test (F–I,K,L): **p* <0.05, ***p* <0.01, ****p* <0.001. Abbreviations: FFA, free fatty acid; GTT, glucose tolerance test; HFD, high-fat diet; ITT, insulin tolerance test; IdIL-2, low-dose IL-2; NCD, normal chow diet; pAkt, phosphorylated Akt; TC, total cholesterol; TG, triglyceride; Treg, regulatory T cell.

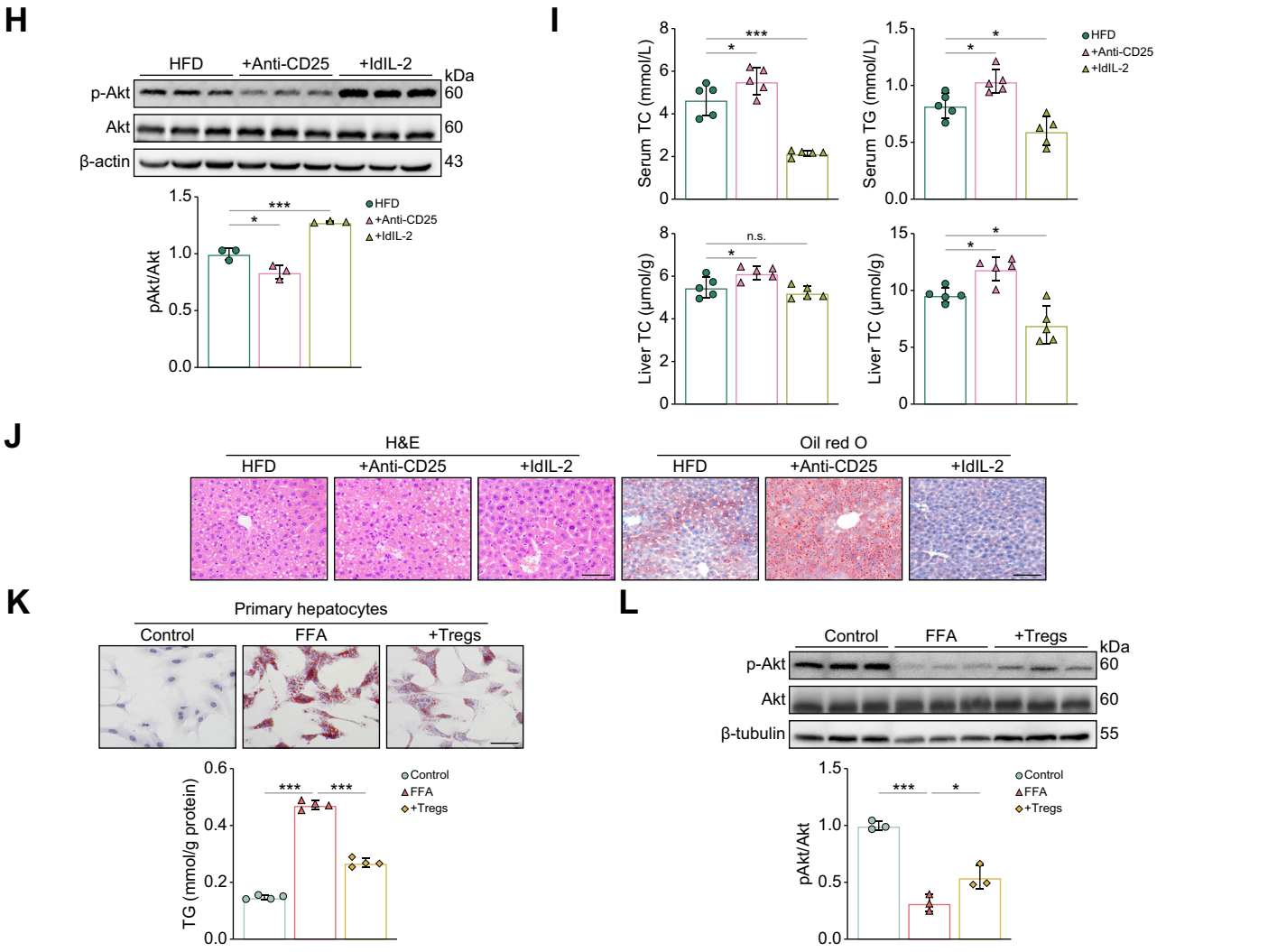

Fig. 1. (*continued*).

and triglyceride (TG) levels in the serum and liver were significantly decreased in Treg-expanded mice compared with HFD mice, whereas these indicators displayed the opposite trend in Treg-depleted mice (Fig. 1I). Accordingly, H&E and Oil red O staining of liver sections also reflected significant lipid accumulation in Treg-depleted mice, an effect that was markedly attenuated in Treg-expanded mice (Fig. 1J). These results suggested that Tregs influence both hepatic lipid homeostasis and IR.

Tregs are one of the major sources of IL-10 within the liver,[26] which is an important protective factor against diet-induced hepatic steatosis and IR.[27] ELISA results showed increased IL-10 production and reduced levels in Treg-depleted mice compared with HFD mice (Fig. S3A). Isolation of Tregs (Fig. S3B) and their co-culture assays with primary hepatocytes showed that Tregs significantly reduced free fatty acid (FFA)-induced lipid accumulation (Fig. 1K) and enhanced insulin-induced pAkt levels in hepatocytes (Fig. 1L). Neutralization of IL-10 confirmed that the ability of Tregs to ameliorate IR and reduce lipid deposition in hepatocytes was IL-10 dependent (Fig.S3C-F).

Aberrant activation of hepatic macrophage Notch1 signaling occurs in parallel with reduced hepatic Treg frequency in hepatic steatosis

To address the reduction in hepatic Treg frequency, we interrogated the GEO database (GEO: GSE83452) and noted that the reduction in Tregs was accompanied by an increase in the proinflammatory macrophage population in patients with MASLD (Fig. S4A). Given the important role of Notch1 signaling in the proinflammatory transformation of macrophages, we examined the activation levels of Notch1 (Notch1 intracellular domain; NICD) in hepatic macrophages of patients with simple steatosis. Immunofluorescence (IF) staining of liver sections from patients with hepatic steatosis revealed that Notch1 activation was increased and predominantly located in macrophages compared with normal samples (Fig. 2A). Subsequently, we

monitored the level of hepatic macrophage Notch1 activation during hepatic steatosis in mice by western blot and flow cytometry. Mice fed a HFD showed a significant and sustained increase in Notch1 activation in hepatic macrophages from 1 to 6 weeks of a HFD diet, compared to the NCD group (Fig. 2B–D). Interestingly, the level of macrophage Notch1 activation was negatively correlated with the frequency of $CD4^+CD25^+Foxp3^+$ Tregs (Fig. 2E). These results suggested that Notch1 signaling activation in hepatic macrophages is involved in the reduced hepatic Treg frequency during the early stage of MASLD.

Deletion of Notch1 in macrophages ameliorates HFD-induced hepatic steatosis and insulin resistance

Next, we investigated the role of macrophage Notch1 in hepatic steatosis by feeding $Notch1^{M\text{-}KO}$ mice and $Notch1^{FL/FL}$ mice with HFD for 6 weeks. $Notch1^{M\text{-}KO}$ mice showed significantly slower body weight gain (Fig. S4C) compared with $Notch1^{FL/FL}$ mice. In addition, compared with $Notch1^{FL/FL}$ mice fed a HFD, Notch1 deficiency showed enhanced glucose tolerance and insulin sensitivity, as determined by GTT and ITT, respectively

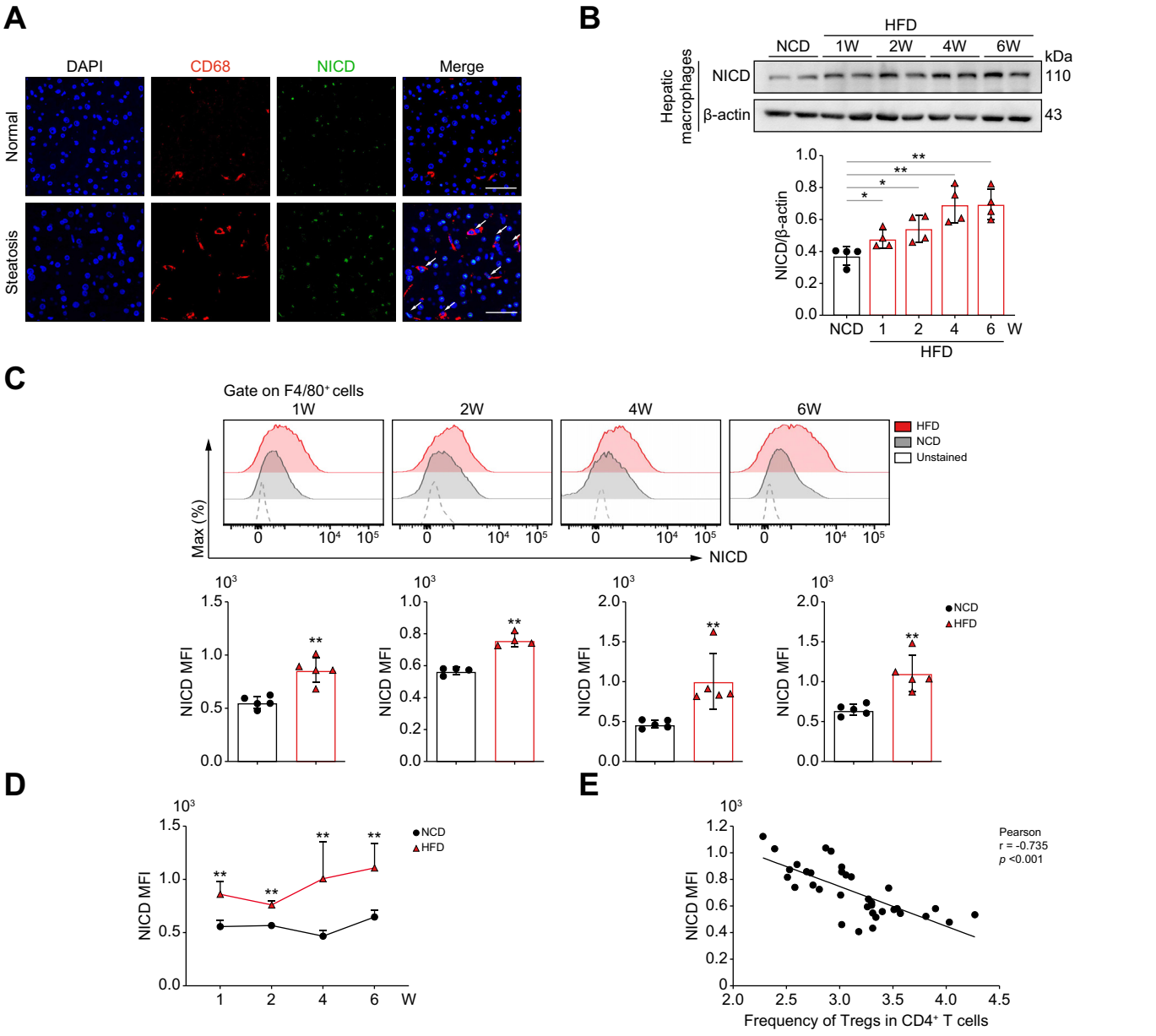

Fig. 2. Hepatic macrophage Notch1 activation is negatively correlated with the frequency of hepatic $CD4^+CD25^+Foxp3^+$ Tregs in hepatic steatosis. (A) Representative pictures of IF staining for NICD in $CD68^+$ cells from liver tissues of patients with or without hepatic steatosis (scale bar: 50 μm). WT C57BL/6 mice were fed with NCD or HFD. (B) Western blot analysis of NICD expression in hepatic macrophages isolated from mice fed a NCD or HFD (four 4/group). (C) Notch1 activation in hepatic macrophages was examined by flow cytometry at different time points (four or five/group). (D) Dynamic changes in the level of Notch1 activation in hepatic macrophages of mice fed a NCD or HFD for 1, 2, 4, and 6 weeks. (E) Relationship between the level of Notch1 activation in hepatic macrophages and frequency of hepatic $CD4^+CD25^+Foxp3^+$ Tregs (38/group). Values represent means ± SD. Statistical analysis was performed by a 2-tailed unpaired Student *t* test: **p* <0.05, ***p* <0.01. Abbreviations: HFD, high-fat diet; IF, immunofluorescence; MFI, mean fluorescence intensity; NCD, normal chow diet; NICD, Notch1 intracellular domain; Treg, regulatory T cell; WT, wild-type.

(Fig. 3A,B). In addition, serum TG, TC, and LDL cholesterol (LDL-C) were largely reduced, and HDL cholesterol (HDL-C) was slightly increased in Notch1$^{M\text{-}KO}$ mice (Fig. 3C). Consistent with these results, hepatic TG was significantly lower in Notch1$^{M\text{-}KO}$ mice, whereas there were no differences in hepatic TC (Fig. 3D). Similarly, H&E and Oil Red O staining of liver sections also confirmed less hepatic steatosis in Notch1$^{M\text{-}KO}$ mice compared with Notch1$^{FL/FL}$ mice (Fig. 3E). Moreover, Notch1 deficiency enhanced the insulin-stimulated hepatic pAkt level, revealing the improvement of hepatic IR in HFD-fed mice (Fig. 3F). Given that inflammation has a primary role in the etiology of hepatic IR, we measured the levels of proinflammatory (TNF-α and IL-1β) and anti-inflammatory [IL-10 and transforming growth factor (TGF)-β] cytokines in liver tissues, finding that Notch1 deficiency reduced the former and elevated the latter. Consistency changes were also found in the percentage of proinflammatory M1 (F4/80^{+}CD11c^{+}) macrophages and anti-inflammatory M2 (F4/80^{+}CD206^{+}) macrophages (Figs. S4D and E).

Tregs are required to reverse HFD-induced hepatic steatosis and insulin resistance in Notch1$^{M\text{-}KO}$ mice

Next, to confirm the correlation between the activation of hepatic macrophage Notch1 signaling and the Treg population, we analyzed the frequency of CD4^{+}CD25^{+}Foxp3^{+} Tregs and the mRNA expression of *foxp3* in liver tissues of Notch1$^{FL/FL}$ and Notch1$^{M\text{-}KO}$ mice fed a HFD. Compared with Notch1$^{FL/FL}$ mice, Notch1 deficiency significantly reversed the HFD-induced reduction in Treg frequency (Fig. 4A,B, Fig. S5). Furthermore, we determined whether the ameliorative effects of macrophage Notch1 deficiency on MASLD were related to

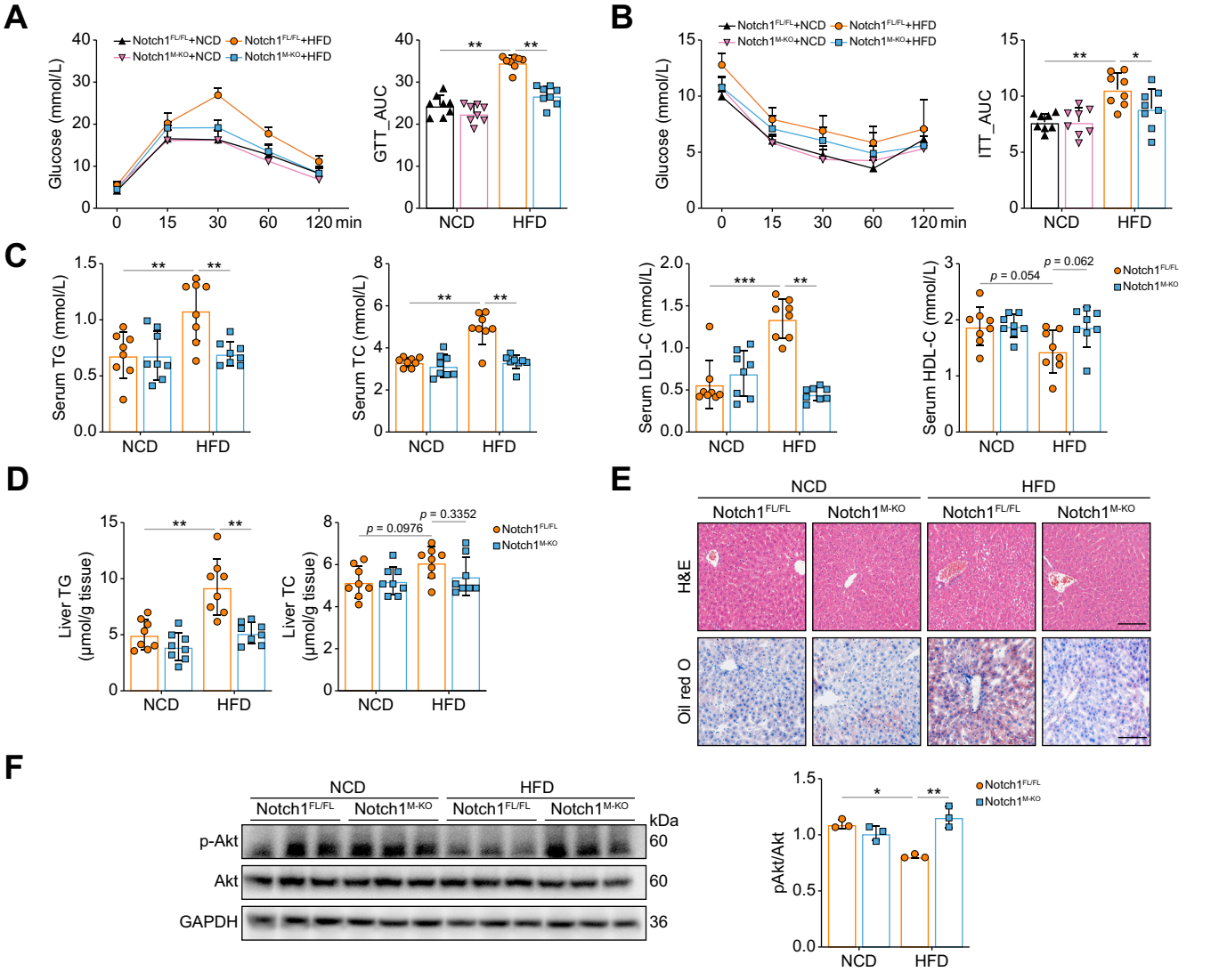

Fig. 3. Deletion of Notch1 in macrophages ameliorates HFD-induced hepatic steatosis and insulin resistance. Notch1$^{FL/FL}$ mice and Notch1$^{M\text{-}KO}$ mice were fed a NCD or HFD for 6 weeks. GTT (A), ITT (B), serum TG, TC, LDL-C, and HDL-C levels (C), and liver TG and TC levels (D) were measured (eight/group). (E) Representative images of H&E and Oil red O staining of liver sections (scale bar: 100 μm). (F) Western blot analyses of insulin-stimulated expression of Akt and pAkt in the liver (three/group). Values represent means ± SD. Statistical analysis was performed by one-way ANOVA and Tukey's test: *p <0.05, **p <0.01, ***p <0.001. Abbreviations: GTT, glucose tolerance test; HDL-C, HDL cholesterol; HFD, high-fat diet; ITT, insulin tolerance test; LDL-C, LDL cholesterol; NCD, normal chow diet; Notch1$^{FL/FL}$, floxed Notch1; Notch1$^{M\text{-}KO}$, myeloid-specific Notch1-knockout; TC, total cholesterol; TG, triglyceride.

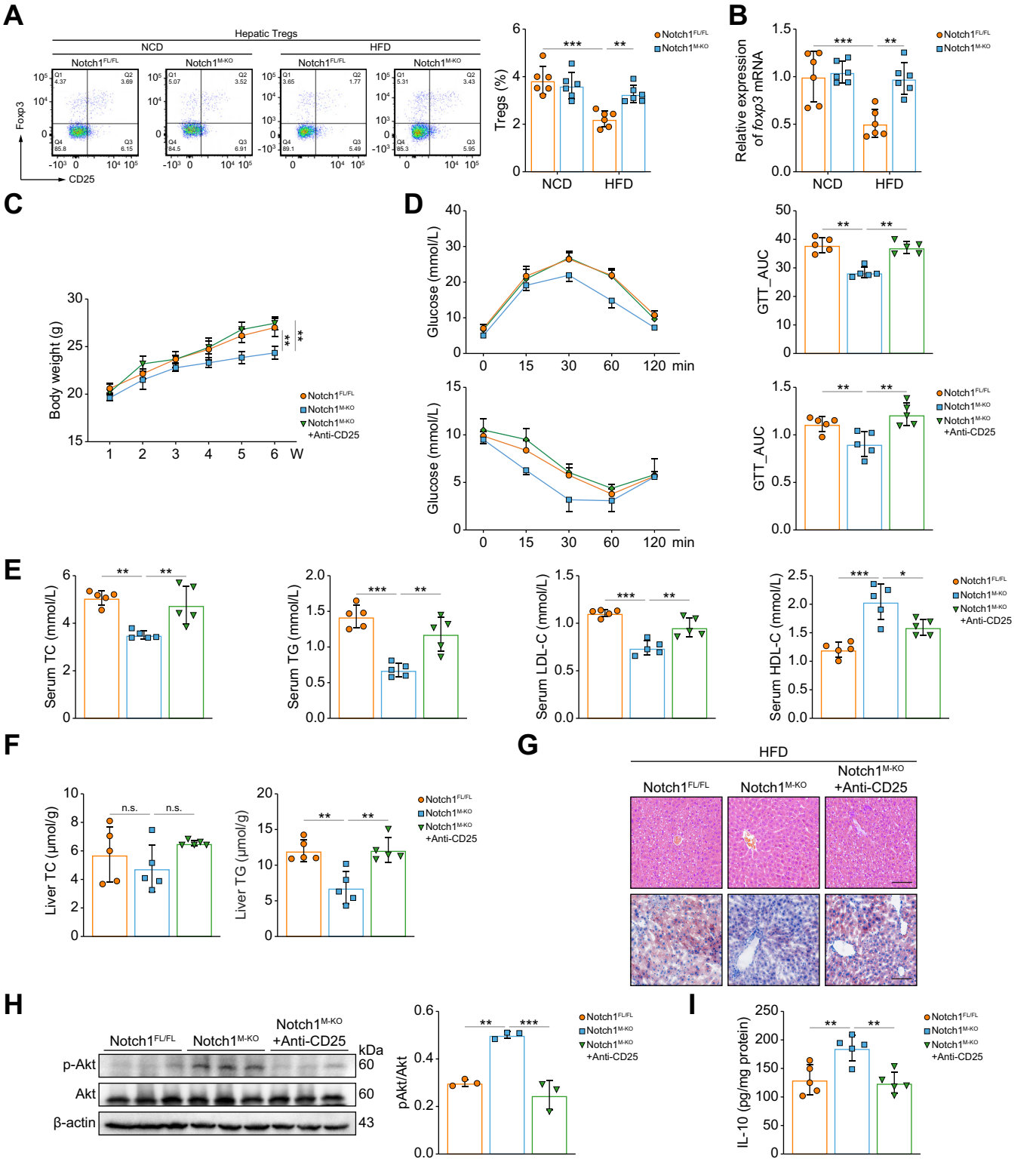

Fig. 4. Improvement effect of Notch1 deficiency in macrophages on hepatic steatosis and insulin resistance is mainly dependent on the increase in Treg frequency. Notch1$^{FL/FL}$ mice and Notch1^{M-KO} mice were fed a NCD or HFD for 6 weeks. (A) Proportion of hepatic CD25^{+}Foxp3^{+} Tregs gated on CD3^{+}CD4^{+} T cells was analyzed by flow cytometry in Notch1$^{FL/FL}$ mice and Notch1^{M-KO} mice (six/group). (B) *Foxp3* mRNA expression in the liver of Notch1$^{FL/FL}$ mice and Notch1^{M-KO} mice (six/group). Notch1$^{FL/FL}$ mice, Notch1^{M-KO} mice, and Notch1^{M-KO} mice with Tregs eliminated (injected intraperitoneally with anti-CD25 antibodies) were fed a HFD for 6 weeks. The body weight (C), GTT, ITT (D), serum TG, TC, LDL-C, and HDL-C levels (E), and liver TG and TC levels (F) were measured (five/group). (G) Representative images of H&E and Oil red O staining of liver sections (scale bar: 100 μm). (H) Western blot analyses of insulin-stimulated expression of Akt and pAkt in the liver (three/group). (I) The level of IL-10 in the liver was measured by ELISA (five/group). Values represent means ± SD. Statistical analysis was performed by one-way ANOVA and Tukey's test. *p <0.05, **p <0.01, ***p <0.001. Abbreviations: GTT, glucose tolerance test; HDL-C, HDL cholesterol; HFD, high-fat diet; ITT, insulin tolerance test; LDL-C, LDL cholesterol; NCD, normal chow diet; Notch1$^{FL/FL}$, floxed Notch1; Notch1^{M-KO}, myeloid-specific Notch1-knockout; TC, total cholesterol; TG, triglyceride; Treg, regulatory T cell.

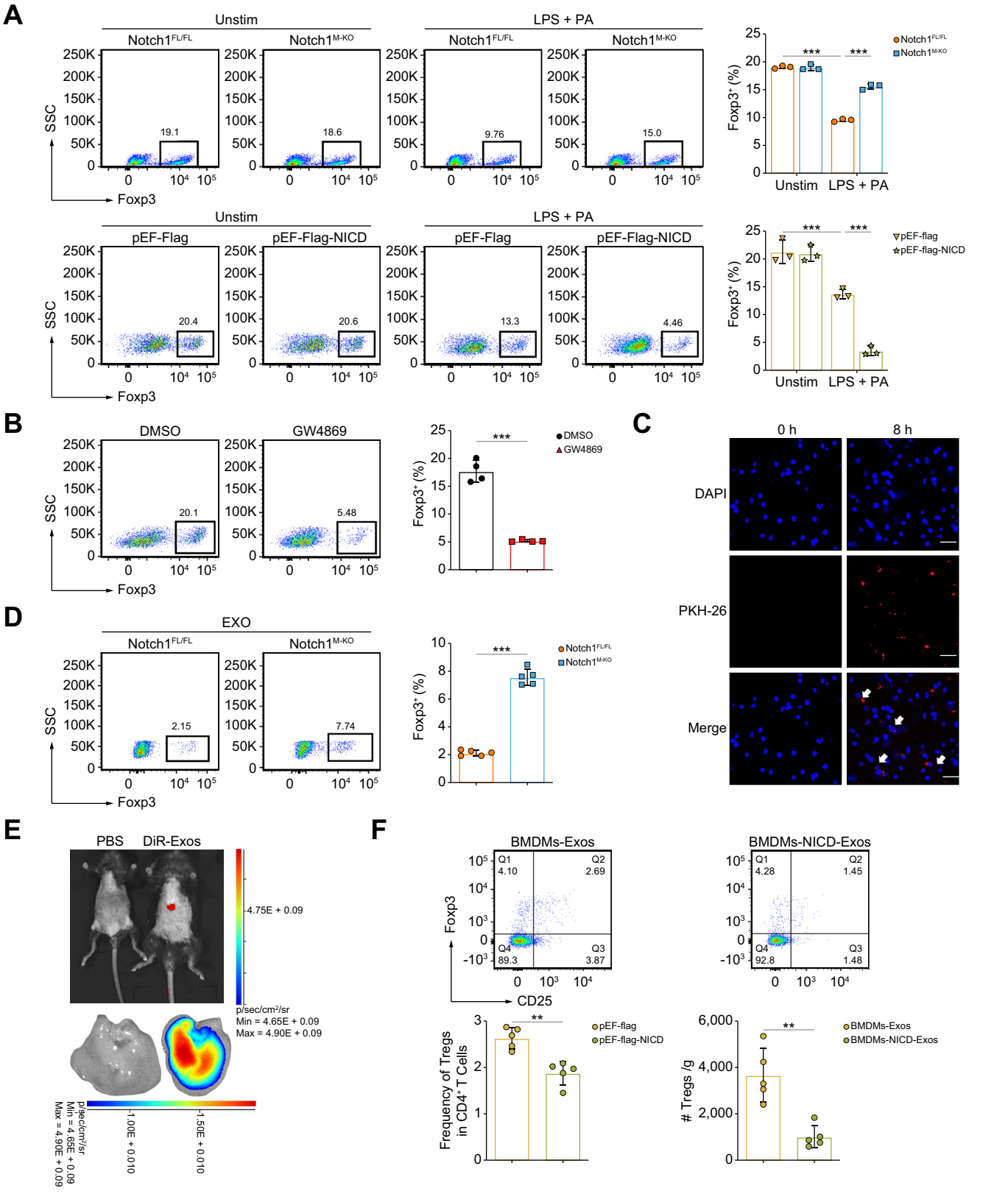

Fig. 5. Exos from Notch1-activated macrophages impede Treg differentiation. BMDMs from Notch1$^{FL/FL}$ and Notch1^{M-KO} mice and pEF-Flag-NICD or pEF-Flag transfected BMDMs were stimulated with LPS (100 ng/ml) and PA (250 μM) or PBS for 12 h and then co-cultured with naïve CD4$^+$ T cells for 3 days. (A) Induction of Foxp3$^+$ Tregs was analyzed by flow cytometry (three/group). (B) Naïve CD4$^+$ T cells were co-cultured with BMDMs treated with GW4869 (5 μM) for 3 days, and the induction of Foxp3$^+$ Tregs was detected by flow cytometry (four/group). (C) BMDM-Exos were labeled with PKH26 (red) and then co-cultured with naïve CD4$^+$ T cells for 8 h. The resulting T cells were collected for fluorescence confocal microscopy to detect Exo uptake and their nuclear location was determined by DAPI (blue) staining (scale bar: 25 μm). (D) BMDMs from Notch1$^{FL/FL}$ and Notch1^{M-KO} mice were stimulated with LPS (100 ng/ml) and PA (250 μM) for 12 h. Naïve CD4+ T cells were

Treg frequency changes by abolishing Tregs in Notch1^{M-KO} mice fed a HFD. Elimination of Tregs significantly increased the body weight (Fig. 4C), systemic IR (Fig. 4D), serum lipid levels (TC, TG, LDL, but not HDL) (Fig. 4E), and intrahepatic lipid content (Fig. 4F,G), but dramatically decreased pAkt and IL-10 (Fig. 4H,I) levels in the liver of Notch1^{M-KO} mice, suggesting that these phenotypes associated with the deletion of Notch1 in macrophages were substantially offset by Treg elimination. Together, these results imply that the ameliorating effect of Notch1 depletion in macrophages on hepatic steatosis and IR is largely dependent on the increased frequency of Tregs.

Exos from Notch1-activated macrophages impede Treg differentiation

Given that the liver is the main source of peripherally induced Tregs derived from naïve CD4$^+$ T cell differentiation, we proposed the hypothesis that Notch1 activation in hepatic macrophages impedes Treg differentiation in hepatic steatosis. To test this hypothesis, an *in vitro* BMDM/naïve CD4$^+$ T cell co-culture system was established (Fig. S6A). BMDMs were stimulated with lipopolysaccharide (LPS) + palmitic acid (PA) (the main stimulating factors of hepatic macrophages in hepatic steatosis) for 12 h, resulting in a significant increase in Notch1 activation (Fig. S6B). CD4$^+$ T cells were harvested 3 days after the co-culture to analyze Foxp3$^+$ Treg frequency by flow cytometry. After LPS+PA treatment, the induction of Foxp3$^+$ Tregs was decreased significantly compared with those of unstimulated cells (Fig. 5A). Strikingly, BMDMs from Notch1^{M-KO} mice exhibited higher induction of Foxp3$^+$ Tregs. Subsequently, we overexpressed NICD in BMDMs through transfection of NICD overexpression plasmids (Fig. S5C). Induction of Foxp3$^+$ Tregs was further reduced in response to overexpression of NICD in BMDMs (Fig. 5A). Consistent with this finding, IF staining also showed that the inducible Foxp3$^+$ Tregs population was markedly enhanced following Notch1 KO and further reduced following NICD overexpression (Fig. S6D).

Exos are an effective mechanism of intercellular communication in the liver.[28] Consequently, we sought to determine whether Exos mediated the effect of macrophages on Treg differentiation. BMDMs were pretreated with GW4869, a commonly used chemical inhibitor that blocks the release of Exos. The inducible effect of BMDMs on Treg differentiation was significantly blunted after GW4869 treatment (Fig. 5B). To further define the molecular effects of BMDM-Exos on Treg differentiation, we isolated Exos from BMDMs and characterized them by transmission electron microscopy and flow nanoanalysis. The vesicles exhibited a cup- or sphere-shaped morphology with a 40–150 nm diameter (Figs. S7A and B). In addition, the Exo marker proteins CD63, CD9, and TSG101 were detected in the BMDM-Exos (Fig. S7C). These results confirmed that Exos were successfully extracted. Next, we examined whether these BMDM-Exos could be taken up by naïve CD4$^+$ T cells. We labeled BMDM-Exos with the red fluorescent dye PKH26 and then added them into the culture medium of naïve CD4$^+$ T cells. After 8 h, confocal microscopy analysis showed that the labeled Exos were efficiently taken up by naïve CD4$^+$ T cells (Fig. 5C). Furthermore, we explored whether the Exos mediated the regulation of macrophagic Notch1 signaling on Treg differentiation. We incubated naïve CD4$^+$ T cells with Exos isolated from LPS+PA-treated Notch1$^{FL/FL}$-BMDMs and Notch1^{M-KO}-BMDMs. Compared with the Notch1$^{FL/FL}$ group, the frequency of Tregs was increased significantly in the Notch1^{M-KO} group (Fig. 5D).

To confirm the effect of macrophage-derived Exos on hepatic Tregs *in vivo*, we tracked the distribution of Exos after tail vein injection and found liver enrichment within 6 h (Fig. 5E). Exos from NICD-transfected BMDMs, stimulated by LPS + PA, were injected into HFD-fed mice, and flow cytometry showed a significant reduction in hepatic Tregs compared with controls (Fig. 5F). Collectively, these data indicated that Notch1 activation in macrophages impedes Treg production via Exos.

Notch1-activated macrophages impede Treg differentiation *via* exosomal miR-142a-3p

To decipher how the Exos from Notch1-activated macrophages affect Treg differentiation, we further analyzed the miRNA expression profiles in Exos from LPS+PA-treated Notch1^{M-KO}-BMDMs compared with those in Exos from Notch1$^{FL/FL}$-BMDMs exposed to the same treatment. miRNA sequencing results indicated that there were 335 miRNAs in common among the two groups (Fig. 6A). The volcano plots and heat maps displayed remarkable differences in miRNA profiles between Notch1^{M-KO}-Exos and Notch1$^{FL/FL}$-Exos (Fig. 6B,C). Among these differentially significantly expressed miRNAs, miR-142a-3p was reported to target TGF-β receptor 1 (TGFBR1) in both human and mouse,[29,30] which is closely associated with Treg differentiation.[31] Subsequently, we validated the change in miR-142a-3p in Exos by RT-qPCR, which was consistent with the miRNA sequencing results. Furthermore, we also found that miR-142a-3p was significantly decreased in CD4$^+$ T cells co-cultured with Notch1^{M-KO}-BMDM-Exos, compared with that in Notch1$^{FL/FL}$-BMDM group (Fig. 6D). These results indicated that Notch1 activation in macrophage-modulated Exo-miR-142a-3p was transferred to CD4$^+$ T cells.

To confirm the effect of miR-142a-3p on Treg differentiation, naïve CD4$^+$ T cells were transfected with an miR-142a-3p inhibitor, mimic, or negative control (NC), and then all cells were co-cultured with BMDMs stimulated with LPS+PA or not. With confirmation of successful transfection (Fig. S8A), we found that the miR-142a-3p mimic significantly inhibited the induction

co-cultured with BMDM-Exos for 3 days, and induction of Foxp3$^+$ Tregs was detected by flow cytometry (five/group). (E) Small animal *in vivo* imaging was used to detect the distribution of DiR-labeled Exo fluorescence signals *in vivo*. (F) Exos were extracted from BMDMs transfected with pEF-Flag-NICD or pEF-Flag after LPS + PA stimulation, and their concentrations were measured using BCA. BMDM-Exos at a dose of 200 μg/mouse were injected via the tail vein into mice fed a HFD for 1 week, followed by another week of HFD feeding. Flow cytometry was used to detect the proportion and number of intrahepatic Tregs mice. Values represent means ± SD. Statistical analysis was performed by (A) one-way ANOVA and Tukey's test or (B,D) 2-tailed unpaired Student *t* test. ***p <0.001. Abbreviations: BMDM, bone marrow-derived macrophage; Exo, exosome; LPS, lipopolysaccharide; NICD, Notch1 intracellular domain; Notch1$^{FL/FL}$, floxed Notch1; Notch1^{M-KO}, myeloid-specific Notch1-knockout; PA, palmitic acid; Treg, regulatory T cell.

of Tregs (Fig. 6E), whereas the miR-142a-3p inhibitor enhanced the induction of Tregs, compared with the corresponding NC (Fig. 6F). More importantly, the inhibition of Tregs induced by overexpressing NICD in macrophages was reversed when $CD4^+$ T cells were transfected with the miR-142a-3p inhibitor (Fig. 6G). Overall, these results suggested that Notch1 activation in macrophages impedes Treg differentiation through Exo-miR-142a-3p.

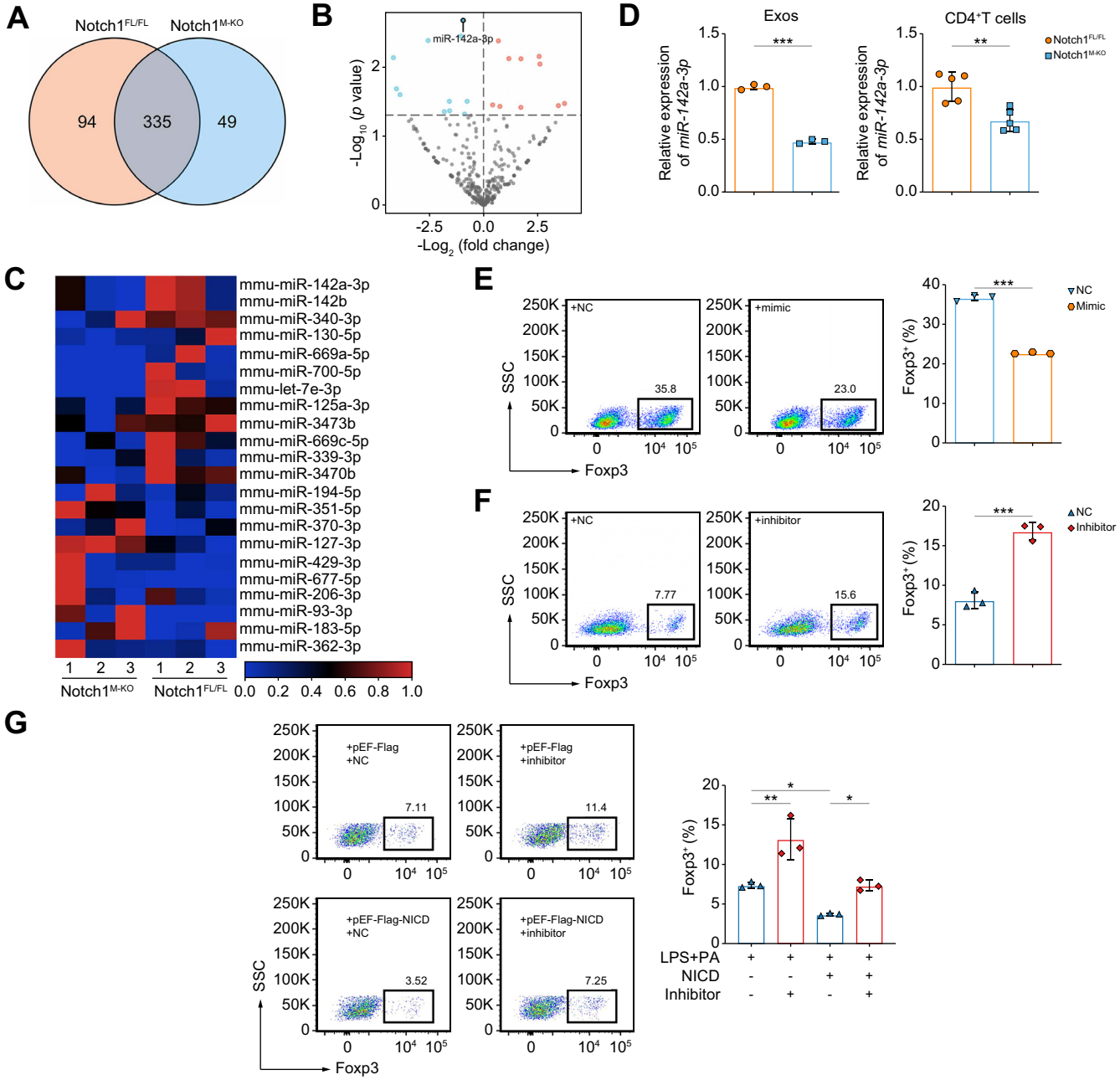

Fig. 6. Exo-miR-142a-3p from Notch1-activated macrophages impedes Treg differentiation. BMDMs from Notch1$^{FL/FL}$ and Notch1^{M-KO} mice were stimulated with LPS (100 ng/ml) and PA (250 μM) for 12 h. The miRNA expression profiles in BMDM-Exos were analyzed by miRNA sequencing (three/group). (A) Venn diagram showing miRNAs in both groups. (B) Volcano plot of differentially expressed miRNAs in both groups. (C) Heatmap of miRNAs that differed significantly (p <0.05) between the groups. (D) Validation of the expression of miR-142a-3p in BMDM-Exos (left panel) (three/group) and $CD4^+$ T cells (right panel) (five/group) between the two groups by RT-qPCR analysis. (E) Induction of $Foxp3^+$ Tregs was detected by flow cytometry after naïve $CD4^+$ T cells transfected with NC or miR-142a-3p mimic were co-cultured with BMDMs (three/group). (F) Induction of $Foxp3^+$ Tregs was detected by flow cytometry after naïve $CD4^+$ T cells transfected with NC or miR-142a-3p-inhibitor were co-cultured with BMDMs pretreated with LPS (100 ng/ml) and PA (250 μM) for 12 h (three/group). (G) pEF-Flag-NICD or pEF-Flag transfected BMDMs were stimulated with LPS (100 ng/ml) and PA (250 μM) or PBS for 12 h, respectively, and then co-cultured with naïve $CD4^+$ T cells transfected with NC or miR-142a-3p-inhibitor for 3 days. The induction of $Foxp3^+$ Tregs was analyzed by flow cytometry (three/group). Values represent means ± SD. Statistical analysis was performed by (D–F) 2-tailed unpaired Student t test or (G) one-way ANOVA and Tukey's test: *p <0.05, **p <0.01, ***p <0.001. Abbreviations: BMDM, bone marrow-derived macrophage; Exo, exosome; LPS, lipopolysaccharide; NC, negative control; NICD, Notch1 intracellular domain; Notch1$^{FL/FL}$, floxed Notch1; Notch1^{M-KO}, myeloid-specific Notch1-knockout; PA, palmitic acid; RT-qPCR, quantitative reverse transcription PCR; Treg, regulatory T cell.

Notch1-induced miR-142a-3p impedes Treg differentiation by targeting TGFBR1

To confirm the target gene of miR-142a-3p, we constructed a wild-type (WT) TGFBR1 3′-untranslated region (UTR) plasmid, as well as a control plasmid in which the miR-142a-3p binding site of the TGFBR1 3′UTR was mutated for use in a luciferase reporter assay (Fig. 7A, Fig. S8B). TGFBR1 3′UTR activities were significantly inhibited by miR-142a-3p-mimic transfection compared with cells transfected with NC, indicating that this 3′UTR is subject to miR-142a-3p regulation (Fig. 7A). Furthermore, we evaluated the effect of miR-142a-3p on the expression of TGFBR1 on CD4$^+$ T cells co-cultured with BMDMs by flow cytometry. Overexpression of miR-142a-3p significantly decreased the expression of TGFBR1 on CD4$^+$ T cells co-cultured with BMDMs (Fig. 7B), whereas miR-142a-3p inhibition increased TGFBR1 expression on CD4+ T cells co-cultured with LPS+PA-treated BMDMs compared with the NC group (Fig. 7C).

Next, to further confirm that the effect of macrophage Notch1 signaling on Treg differentiation is mediated by TGFBR1, the expression of TGFBR1 in CD4$^+$ T cells co-cultured with BMDMs was determined. The expression of TGFBR1 markedly increased in CD4$^+$ T cells co-cultured with LPS+PA-treated Notch1$^{M\text{-}KO}$-BMDMs compared with the Notch1$^{FL/FL}$ group, and was markedly reduced when Notch1 was overexpressed in BMDMs (Fig. 7D,E). In addition, in Notch1$^{M\text{-}KO}$ mice fed a HFD, macrophage Notch1 deficiency

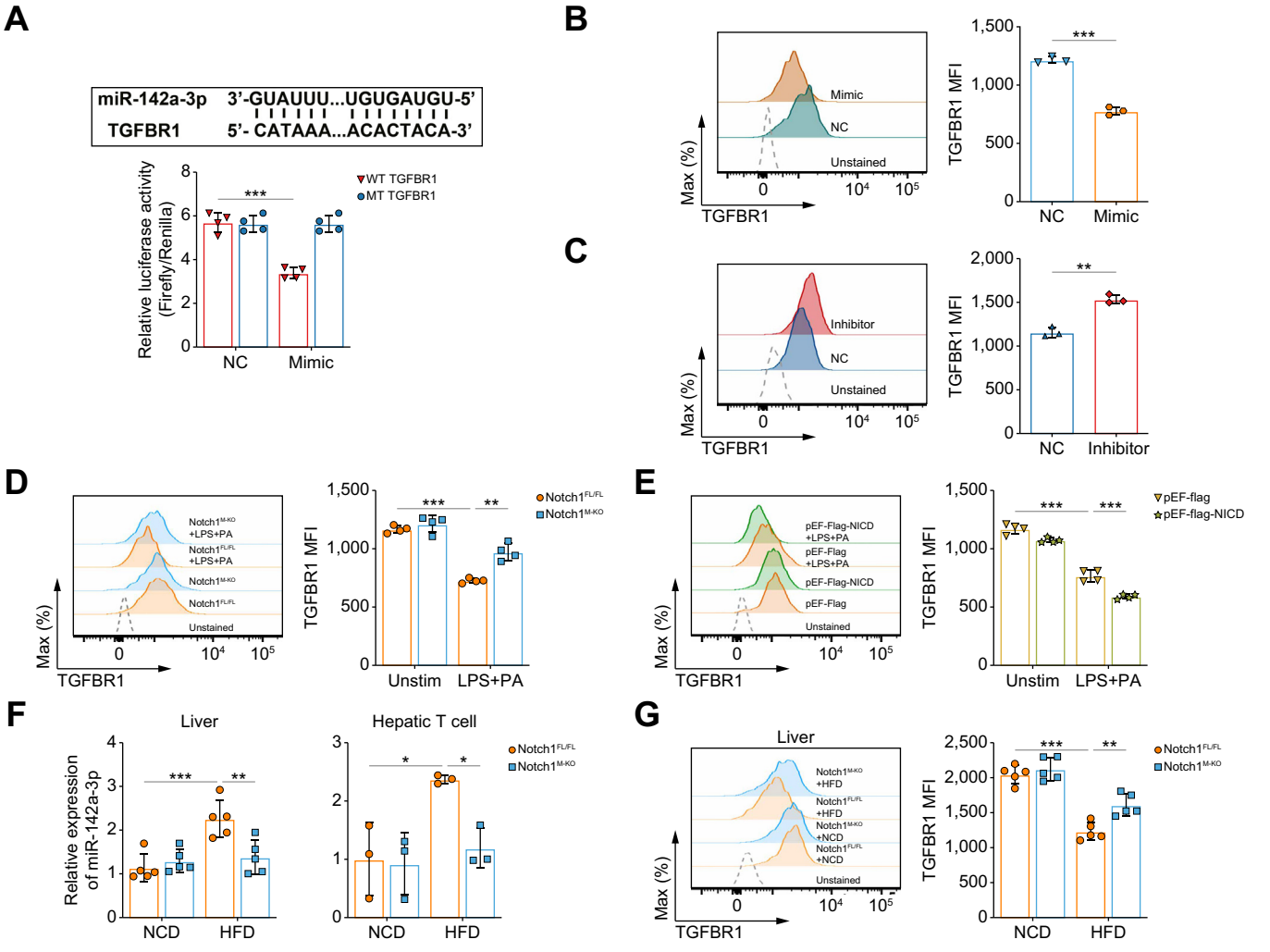

Fig. 7. Notch1-induced miR-142a-3p impedes Treg differentiation by targeting TGFBR1. (A) Prediction of the binding site of miR-142a-3p in *TGFBR1* by miRWalk and miRDB (upper panel) and luciferase assay revealing binding of miR-142a-3p to the TGFBR1 3′UTR (lower panel). MFI of TGFBR1 in T cells was detected by flow cytometry after (B) naïve CD4$^+$ T cells transfected with NC or a miR-142a-3p mimic were co-cultured with BMDMs (three/group), (C) naïve CD4$^+$ T cells transfected with NC or miR-142a-3p inhibitor were co-cultured with BMDMs pretreated with LPS (100 ng/mL) and PA (250 μM) for 12 h (three/group), (D) naïve CD4$^+$ T cells co-cultured with BMDMs from Notch1$^{FL/FL}$ and Notch1$^{M\text{-}KO}$ mice pretreated with LPS (100 ng/ml) and PA (250 μM) or PBS for 12 h (four/group), and (E) naïve CD4$^+$ T cells co-cultured with LPS (100 ng/ml) and PA (250 μM) or PBS-pretreated BMDMs transfecting pEF-Flag-NICD or control plasmids for 12 h (four/group). The level of miR-142a-3p (F) and MFI of TGFBR1 in CD4$^+$ T cells (G) in the liver tissues of Notch1$^{FL/FL}$ mice and Notch1$^{M\text{-}KO}$ mice fed with NCD or HFD for 6 weeks (five/group) were detected. Values represent means ± SD. Statistical analysis was performed by (A, D–G) one-way ANOVA and Tukey's test, or (B, C) 2-tailed unpaired Student *t* test. ***p* <0.01, ****p* <0.001. Abbreviations: BMDM, bone marrow-derived macrophage; HFD, high-fat diet; LPS, lipopolysaccharide; MFI, mean fluorescence intensity; NC, negative control; NCD, normal chow diet; NICD, Notch1 intracellular domain; Notch1$^{FL/FL}$, floxed Notch1; Notch1$^{M\text{-}KO}$, myeloid-specific Notch1-knockout; PA, palmitic acid; TGFBR1, transforming growth factor beta receptor 1; UTR, untranslated region.

decreased miR-142a-3p levels in the liver and hepatic T cells and increased TGFBR1 expression in hepatic CD4$^+$ T cells compared with Notch1$^{FL/FL}$ mice (Fig. 7F,G). Collectively, these results suggest that Notch1 signaling in macrophages regulates miR-142a-3p, which subsequently affects the expression of TGFBR1 on CD4$^+$ T cells, leading to a decrease in Tregs.

Discussion

The role of Tregs in suppressing local inflammation has been extensively investigated,[32] and emerging reports have highlighted their function in modulating non-immune lineages to maintain tissue homeostasis.[33,34] In the present study, we identified that decreased Tregs contributed to HFD-induced hepatic steatosis and IR during the early stage of MASLD. Our results are consistent with prior work on hepatic Tregs, in which hepatic Treg frequency showed a significant decrease in mice after 1 week of a HFD and continued to decrease throughout the HFD feeding period.[35] Furthermore, our results showed that hepatic Treg depletion significantly exacerbated lipid accumulation and IR. In agreement with this, a previous RNA-sequencing study demonstrated substantial changes in the expression of hepatic genes regulating lipid metabolism following Treg depletion.[36] In addition, Tregs in visceral adipose tissue have been shown to have a clear insulin-sensitizing function,[37] with adoptive Treg transfer also decreasing adipocyte size in mouse models of obesity.[38] However, increasing the frequency of Tregs only in subcutaneous adipose tissue but not in the liver can exacerbate hepatic steatosis,[39] a phenomenon that might result from organ crosstalk. In this study, ldIL-2 treatment was used to achieve hepatic Treg amplification, which significantly reduced hepatic steatosis. This suggests that attention should be paid to whether Tregs can be specifically enriched in liver tissue during the expansion of Tregs as part of *in vivo* therapy for liver diseases. Hepatic Tregs suppress MASH by alleviating intrahepatic inflammation,[8] whereas they promote tumor development during the premalignant stage of MASH livers,[9] which suggest that the effect of hepatic Tregs varies in response to various stimuli and the corresponding microenvironment during different stages of disease (early or late).

Environmental signals in peripheral tissues favor the development of antigen-specific Tregs. It is well documented that the activation status of macrophages in tissues is tightly connected to Treg homeostasis. For example, tumor-associated macrophages induce the imbalance of Tregs and T helper type 17 cells (Th-17),[40] and the proinflammatory macrophages of visceral adipose tissue in obesity can cause Th17/Treg imbalance in visceral adipose tissue.[41] In this study, increased Notch1 activation in hepatic macrophages was synchronized with the reduced hepatic Treg frequency in HFD-induced mice with hepatic steatosis. Additionally, our *in vivo* data revealed that deletion of Notch1 in macrophages reversed the HFD-induced reduction in hepatic Treg frequency, which was accompanied by improvements in hepatic steatosis and IR, largely attributed to changes in Treg frequency. Previous studies on Treg differentiation have primarily focused on the intrinsic role of Notch1 signaling in T cells;[42,43] however, our study revealed that Notch1 signaling in macrophages could regulate macrophage–T cell interactions, highlighting the importance of cell-specific activities of Notch1 in different cell types.

Exos have been emerged as crucial mediators of intercellular communication and are involved in various pathological processes, including liver diseases, as well as carrying and delivering miRNAs, proteins, and metabolites from host to recipient cells.[16] Previous work in MASH has noted the importance of Exo-mediated cellular communication between hepatic macrophages and other cells.[44] The present study identified that macrophage-derived Exos could be taken up by naïve CD4$^+$ T cells and perform a regulatory function on Treg differentiation. Notch1-deficient macrophages significantly improved the induction of Tregs by Exos secreted by LPS+PA-treated macrophages, suggesting that Exos are an important pathway for macrophage Notch1 signaling involved in regulating Treg differentiation. Exo-mediated miRNA transfer is important in various processes, including immune homeostasis.[45] Multiple miRNAs have been identified to be involved in regulating Treg generation and function.[46] In addition, Notch1 signaling has been reported to regulate miRNA expression.[18,19] Further Exo-miRNA sequencing and functional studies demonstrated that macrophage Notch1 signaling regulating Treg differentiation might depend on an Exo-miR-142a-3p–TGFBR1 pathway. TGFBR1 serves as a crucial receptor in TGF-β signaling, which is required for the induction of Tregs.[47] Kimura et al. revealed that the targeted silence of TGFBR1 in naïve CD4$^+$ T cells inhibited the differentiation of Tregs.[31] Our study demonstrated that Notch1 deletion in macrophages reduced the levels of miR-142a-3p, increased TGFBR1 expression on CD4$^+$ T cells, and enhanced Treg frequency both *in vitro* and *in vivo*. These findings suggest that decreased Treg levels during the early stage of MASLD result from macrophages with aberrant Notch1 activation releasing miR-142a-3p, which inhibits the expression of TGFBR1 on CD4$^+$ T cells, thereby impeding Treg production.

In conclusion, this study highlights the crucial role of hepatic Tregs during the early stage of MASLD and identifies a previously unrecognized molecular mechanism of a macrophage Notch1/exo-miR-142a-3p/TGFBR1 pathway in regulating Treg differentiation. Although we cannot rule out that macrophage Notch1 activation might regulate Treg production through pathways other than Exos, our findings provide evidence of the involvement of Exos in the crosstalk between macrophages and CD4$^+$ T cells. However, because we focused exclusively on the early stage of MASLD, our findings might not be readily extended to MASH or fibrotic stages. Nevertheless, this study expands our current understanding of the role of crosstalk between immune cell populations in MASLD. Moreover, our findings provide rationale for a potential immunological approach for the treatment of MASLD by the induction of Tregs.

Affiliations

[1]*Department of Pharmacology, Wuhan University TaiKang Medical School (School of Basic Medical Sciences), Wuhan 430071, China;* [2]*Department of Hepatobiliary and Pancreatic Surgery, Hubei Provincial Clinical Medicine Research Center for Minimally Invasive Diagnosis and Treatment of Hepatobiliary and Pancreatic Diseases, Zhongnan Hospital of Wuhan University, Wuhan 430071, China;* [3]*Department of Physiology, Wuhan University TaiKang Medical School (School of Basic Medical Sciences), Wuhan 430071, China;* [4]*Department of Blood Transfusion, Zhongnan Hospital of Wuhan University, Wuhan, 430071, China*

Abbreviations

BMDM, bone marrow-derived macrophage; Exo, exosome; FFA, free fatty acid; GTT, glucose tolerance test; HDL-C, HDL cholesterol; HFD, high-fat diet; IF, immunofluorescence; IR, insulin resistance; ITT, insulin tolerance test; ldIl-2, low-dose IL-2; LDL-C, LDL cholesterol; LPS, lipopolysaccharide; LysM-Cre, Lyz2-Cre mice; MASH, metabolic dysfunction-associated steatohepatitis; MASLD, metabolic dysfunction-associated steatotic liver disease; MFI, mean fluorescence intensity; NC, negative control; NCD, normal chow diet; NICD, Notch1 intracellular domain; $Notch1^{FL/FL}$, floxed Notch1; $Notch1^{M\text{-}KO}$, myeloid-specific Notch1-knockout; PA, palmitic acid; pAkt, phosphorylation of Akt at S473; RT-qPCR, quantitative reverse transcription PCR; TC, total cholesterol; TG, triglyceride; TGFBR1, transforming growth factor beta receptor 1; TGF-β, transforming growth factor-β; Th17, T helper type 17; Treg, regulatory T cell; UTR, untranslated region; WT, wild-type.

Financial support

This work was supported by the National Nature Science Foundation of China (82173872 and 81872663), the Natural Science Foundation of Hubei Province (2023AFB611), and the Basic-Clinical Medicine Joint Fund of Zhongnan Hospital of Wuhan University (ZNLH202207).

Conflicts of interests

The authors declare no conflicts of interest that pertain to this work. Please refer to the accompanying ICMJE disclosure forms for further details.

Authors' contribution

Analyzed, interpreted the data, and drafted the manuscript: M-YZ, KL. Data collection: X-XH, D-QX, R-BZ, Q-TH, X-YD, Q-YZ, C-CJ, YG. Designed the original study, supervised research, and critically reviewed the paper: CYL, JP. Reviewed the draft for important intellectual content and approved the final article for submission: all authors.

Data availability statement

The miRNA-seq data have been deposited at GEO and are publicly available as of the date of publication. The accession number is PRJNA1046700.

Supplementary data

Supplementary data to this article can be found online at https://doi.org/10.1016/j.jhepr.2024.101242.

References

Author names in bold designate share co-first authorship

[1] Huang DQ, El-Serag HB, Loomba R. Global epidemiology of NAFLD-related HCC: trends, predictions, risk factors and prevention. Nat Rev Gastroenterol Hepatol 2021;18:223–238.
[2] Febbraio MA, Reibe S, Shalapour S, et al. Preclinical models for studying NASH-driven HCC: how useful are they? Cell Metab 2019;29:18–26.
[3] Cai J, Zhang XJ, Li H. The role of innate immune cells in nonalcoholic steatohepatitis. Hepatology 2019;70:1026–1037.
[4] Peiseler M, Schwabe R, Hampe J, et al. Immune mechanisms linking metabolic injury to inflammation and fibrosis in fatty liver disease - novel insights into cellular communication circuits. J Hepatol 2022;77:1136–1160.
[5] Allan SE, Passerini L, Bacchetta R, et al. The role of 2 FOXP3 isoforms in the generation of human $CD4^+$ Tregs. J Clin Invest 2005;115:3276–3284.
[6] Hou X, Song J, Su J, et al. CD4(+)Foxp3(+) Tregs protect against innate immune cell-mediated fulminant hepatitis in mice. Mol Immunol 2015;63:420–427.
[7] **Wu KJ**, **Qian QF**, **Zhou JR**, et al. Regulatory T cells (Tregs) in liver fibrosis. Cell Death Discov 2023;9:53.
[8] Roh YS, Kim JW, Park S, et al. Toll-like receptor-7 signaling promotes nonalcoholic steatohepatitis by inhibiting regulatory T cells in mice. Am J Pathol 2018;188:2574–2588.
[9] Wang H, Zhang H, Wang Y, et al. Regulatory T-cell and neutrophil extracellular trap interaction contributes to carcinogenesis in non-alcoholic steatohepatitis. J Hepatol 2021;75:1271–1283.
[10] Zhang Z, Salgado OC, Liu B, et al. An OGT-STAT5 axis in regulatory T cells controls energy and iron metabolism. Front Immunol 2022;13:874863.
[11] Loomba R, Friedman SL, Shulman GI. Mechanisms and disease consequences of nonalcoholic fatty liver disease. Cell 2021;184:2537–2564.
[12] Carambia A, Freund B, Schwinge D, et al. TGF-beta-dependent induction of CD4(+)CD25(+)Foxp3(+) Tregs by liver sinusoidal endothelial cells. J Hepatol 2014;61:594–599.
[13] Heymann F, Peusquens J, Ludwig-Portugall I, et al. Liver inflammation abrogates immunological tolerance induced by Kupffer cells. Hepatology 2015;62:279–291.
[14] Stienstra R, Saudale F, Duval C, et al. Kupffer cells promote hepatic steatosis via interleukin-1beta-dependent suppression of peroxisome proliferator-activated receptor alpha activity. Hepatology 2010;51:511–522.
[15] **Dong X**, **Feng Y**, Xu D, et al. Targeting macrophagic 17beta-HSD7 by fenretinide for the treatment of nonalcoholic fatty liver disease. Acta Pharm Sin B 2023;13:142–156.
[16] **Sato K**, **Meng F**, Glaser S, et al. Exosomes in liver pathology. J Hepatol 2016;65:213–221.
[17] **Meng W**, **Hao Y**, He C, et al. Exosome-orchestrated hypoxic tumor microenvironment. Mol Cancer 2019;18:57.
[18] Zhao JL, Huang F, He F, et al. Forced activation of Notch in macrophages represses tumor growth by upregulating miR-125a and disabling tumor-associated macrophages. Cancer Res 2016;76:1403–1415.
[19] **Boelens MC**, **Wu TJ**, **Nabet BY**, et al. Exosome transfer from stromal to breast cancer cells regulates therapy resistance pathways. Cell 2014;159:499–513.
[20] Radtke F, MacDonald HR, Tacchini-Cottier F. Regulation of innate and adaptive immunity by Notch. Nat Rev Immunol 2013;13:427–437.
[21] Damle SR, Martin RK, Cockburn CL, et al. ADAM10 and Notch1 on murine dendritic cells control the development of type 2 immunity and IgE production. Allergy 2018;73:125–136.
[22] Ballester-Lopez C, Conlon TM, Ertuz Z, et al. The Notch ligand DNER regulates macrophage IFNgamma release in chronic obstructive pulmonary disease. EBioMedicine 2019;43:562–575.
[23] An L, Li Z, Shi L, et al. Inflammation-targeted celastrol nanodrug attenuates collagen-induced arthritis through NF-kappaB and Notch1 pathways. Nano Lett 2020;20:7728–7736.
[24] Wang X, Sun L, Zhang L, et al. Effect of adoptive transfer or depletion of regulatory T cells on triptolide-induced liver injury. Front Pharmacol 2016;7:99.
[25] Buitrago-Molina LE, Pietrek J, Noyan F, et al. Treg-specific IL-2 therapy can reestablish intrahepatic immune regulation in autoimmune hepatitis. J Autoimmun 2021;117:102591.
[26] Erhardt A, Biburger M, Papadopoulos T, et al. IL-10, regulatory T cells, and Kupffer cells mediate tolerance in concanavalin A-induced liver injury in mice. Hepatology 2007;45:475–485.
[27] Cintra DE, Pauli JR, Araujo EP, et al. Interleukin-10 is a protective factor against diet-induced insulin resistance in liver. J Hepatol 2008;48:628–637.
[28] **Hou X**, **Yin S**, Ren R, et al. Myeloid-cell-specific IL-6 signaling promotes microRNA-223-enriched exosome production to attenuate NAFLD-associated fibrosis. Hepatology 2021;74:116–132.
[29] Chen L, Xiong Y, Hu YQ, et al. Regulatory T cell-exosomal miR-142-3p promotes angiogenesis and osteogenesis via TGFBR1/SMAD2 inhibition to accelerate fracture repair. Chem Eng J 2022;427:131419.
[30] Yang X, Dan X, Men R, et al. MiR-142-3p blocks TGF-beta-induced activation of hepatic stellate cells through targeting TGFbetaRI. Life Sci 2017;187:22–30.
[31] Kimura K, Hohjoh H, Fukuoka M, et al. Circulating exosomes suppress the induction of regulatory T cells via let-7i in multiple sclerosis. Nat Commun 2018;9:17.
[32] Georgiev P, Charbonnier LM, Chatila TA. Regulatory T cells: the many faces of Foxp3. J Clin Immunol 2019;39:623–640.
[33] Panduro M, Benoist C, Mathis D. Tissue Tregs. Annu Rev Immunol May 20 2016;34:609–633.
[34] **Shao Q**, **Gu J**, **Zhou J**, et al. Tissue Tregs and maintenance of tissue homeostasis. Front Cell Dev Biol 2021;9:717903.
[35] Ma X, Hua J, Mohamood AR, et al. A high-fat diet and regulatory T cells influence susceptibility to endotoxin-induced liver injury. Hepatology 2007;46:1519–1529.
[36] Klingenberg R, Gerdes N, Badeau RM, et al. Depletion of $FOXP3^+$ regulatory T cells promotes hypercholesterolemia and atherosclerosis. J Clin Invest 2013;123:1323–1334.
[37] **Meng F**, **Hao P**, Du H. Regulatory T cells differentiation in visceral adipose tissues contributes to insulin resistance by regulating JAZF-1/PPAR-gamma pathway. J Cell Mol Med 2023;27:553–562.

[38] Eller K, Kirsch A, Wolf AM, et al. Potential role of regulatory T cells in reversing obesity-linked insulin resistance and diabetic nephropathy. Diabetes 2011;60:2954–2962.
[39] **Van Herck MA**, **Vonghia L**, Kwanten WJ, et al. Adoptive cell transfer of regulatory T cells exacerbates hepatic steatosis in high-fat high-fructose diet-fed mice. Front Immunol 2020;11:1711.
[40] **Zhou J**, **Li X**, **Wu X**, et al. Exosomes released from tumor-associated macrophages transfer miRNAs that induce a Treg/Th17 cell imbalance in epithelial ovarian cancer. Cancer Immunol Res 2018;6:1578–1592.
[41] Zhang S, Gang X, Yang S, et al. The alterations in and the role of the Th17/Treg balance in metabolic diseases. Front Immunol 2021;12:678355.
[42] Radtke F, Fasnacht N, Macdonald HR. Notch signaling in the immune system. Immunity 2010;32:14–27.
[43] Romero-Wolf M, Shin B, Zhou W, et al. Notch2 complements Notch1 to mediate inductive signaling that initiates early T cell development. J Cell Biol 2020;219:e202005093.
[44] Gao H, Jin Z, Bandyopadhyay G, et al. MiR-690 treatment causes decreased fibrosis and steatosis and restores specific Kupffer cell functions in NASH. Cell Metab. 2022;34:978–990.
[45] Yu MY, Jia HJ, Zhang J, et al. Exosomal miRNAs-mediated macrophage polarization and its potential clinical application. Int Immunopharmacol 2023;117:109905.
[46] Kunze-Schumacher H, Krueger A. The role of microRNAs in development and function of regulatory T Cells - lessons for a better understanding of microRNA biology. Front Immunol 2020;11:2185.
[47] Bronevetsky Y, Burt TD, McCune JM. Lin28b regulates fetal regulatory T cell differentiation through modulation of TGF-beta signaling. J Immunol 2016;197:4344–4350.

Keywords: Hepatic Tregs; Exosomes; Macrophages; Notch1; Hepatic steatosis.
Received 28 March 2024; received in revised form 30 September 2024; accepted 4 October 2024; Available online 11 October 2024

Journal of Hepatology, Volume *7*

Supplemental information

Macrophage Notch1 signaling modulates regulatory T cells via the TGFB axis in early MASLD

Mengya Zhang, Kun Li, Xiaoxing Huang, Dongqin Xu, Ruobin Zong, Qintong Hu, Xiaoyu Dong, Qinyong Zhang, Chaochen Jiang, Yue Ge, Changyong Li, and Jie Ping

Macrophage Notch1 signaling modulates regulatory T cells via the TGFB axis in early MASLD

Mengya Zhang, **Kun Li**, Xiaoxing Huang, Dongqin Xu, Ruobin Zong, Qintong Hu, Xiaoyu Dong, Qinyong Zhang, Chaochen Jiang, Yue Ge, Changyong Li and Jie Ping

Materials and methods 2

Supplementary figures 11

Supplementary tables 19

References 21

Original western blot data 22

Materials and methods

Animal treatment

C57BL/6 mice were obtained from the Experimental Center of Hubei Medical Scientific Academy. Male mice at 8 weeks of age were fed with normal chow diet (NCD, 11.9% kcal fat) or high-fat diet (HFD, 60% kcal fat) (F3282, BioServ, Inc., Frenchtown, NJ) for 1, 2, 4, and 6 weeks. To generate Tregs-expansion mice, mice were injected intraperitoneally once a week with 1μg IL-2 (212-12, Preprotech, Chicago, USA) and 5 μg anti-IL-2 (16-7022-85, eBioscience, Chicago, USA) following HFD feeding. To generate Tregs-depletion mice, mice were given purified anti-CD25 antibody (200 μg) (BE0012, BioXcell, West Lebanon, NH) once a week following HFD feeding. All mice were maintained under standard conditions (25°C, 12-hour light-dark cycle) and had free access to food and water *ad libitum* at the Center for Animal Experiment of Wuhan University (Wuhan, China). All animal protocols were approved by the Committee on the Ethics of Animal Experiments at Wuhan University School of Medicine (Permit No: WP20220219). All mice received humane care in accordance with the criteria outlined in the Guide for the Care and Use of Laboratory Animals.

Human liver specimens

Human liver tissues from patients with simple steatosis and controls were collected by liver biopsy at Zhongnan Hospital of Wuhan University (Wuhan, China). Liver specimens were diagnosed as normal and simple steatosis, which is based on imaging studies and the histological diagnosis of NAFLD. Informed consent was available for each patient. This study was approved by the medical ethics committee of Zhongnan

Hospital of Wuhan University (Ethical Approval Number: 2023022). All research was conducted in accordance with both the Declarations of Helsinki and Istanbul.

Flow cytometry

Isolation of liver nonparenchymal cells of mouse liver was performed using methods previously described[1]. Subsequently, cells were stained with fluorochrome-conjugated antibodies according to the following protocols: (1) For the detection of Tregs frequency, cells were stained with surface antibodies against CD3-FITC (11-0032-82, eBioscience, San Diego, CA, USA), CD4-APC (17-0041-82, eBioscience) and CD25-PeCy7 (25-0251-81, eBioscience) for 30 min at 4°C in the dark. Then, cells were fixed with the Foxp3 Fixation/Permeabilization working solution according to the manufacturer's instruction (00-5523-00, eBioscience) and stained with Foxp3-PE (12-4771-82, eBioscience) for 30 min at RT in the dark. (2) For the detection of Notch1 in macrophages, cells were stained with surface antibody against F4/80-PeCy7 (12-4771-82, eBioscience) for 30 min at 4°C in the dark. After staining, fixation, and permeabilization, an antibody with a specific high affinity for the intracellular domain of Notch1 (12-5785-82, Biolegend, San Diego, CA, USA) was added for 30 min at RT in the dark. (3) To analyze macrophage immunophenotype, cells were stained with surface antibodies against F4/80-PeCy7, CD11c-PE (117308, Biolegend), and CD206-APC (141708, Biolegend) for 30 min at RT in the dark. (4) For the detection of TGFBR1 in $CD4^+$ T cells, cells were stained with surface antibody against CD4-FITC (11-0041-82, eBioscience) for 30 min at 4°C in the dark. After that, cells were fixed and permeabilized where further intracellular staining with TGFBR1 (ab31013, Abcam,

Cambridge, UK) and goat anti-rabbit IgG/PE (bs-0295G-PE, Bioss, Shanghai, China) antibodies were performed.

For the co-culture experiments *in vitro*, after naïve $CD4^+$ T cells were co-cultured with bone marrow-derived macrophages (BMDMs) or Exos from BMDMs, the proportion of Tregs ($Foxp3^+$) and the expression of TGFBR1 on $CD4^+$ T cells were detected by flow cytometry analysis. Cells were stained with surface antibodies against CD4-FITC or TGFBR1 and goat anti-rabbit IgG/PE for 30 min at 4°C in the dark. Subsequently, cells were fixed with the Foxp3 Fixation/Permeabilization working solution and stained with Foxp3-PE for 30 min at RT in the dark. Data were acquired at BD FACS AriaTM III flow cytometer (BD Biosciences, San Jose, USA), equipped with FACS Diva software. All data analysis was performed using FlowJo software (version 10.0.7).

Evaluation of immune cell populations

The ssGSEA algorithm was used to evaluate the immune cell populations in the GSE83452 dataset.

Isolation of Hepatic Macrophages

The hepatic macrophages were isolated as previously described[2], the purity of macrophages was determined by flow cytometry (Figure S4B).

Isolation of Hepatic T cells

Isolation of liver nonparenchymal cells of mouse liver was performed using methods previously described[1]. Subsequently, in a centrifuge tube, 70% Percoll, 40% Percoll, and the single-cell suspension were sequentially layered. The tube was then centrifuged

at 900g for 20 minutes at 4°C, with an acceleration setting of 4 and a deceleration setting of 0. The lymphocyte-enriched layer was collected from between the 40% and 70% Percoll gradients. The purity of macrophages was determined by flow cytometry (Figure S9).

Glucose and insulin tolerance testing (GTT and ITT)

For the GTT, mice were fasted overnight and then given an intraperitoneal injection of glucose (1 g/kg). For the ITT, mice were fasted 5 h, and then given an intraperitoneal injection of insulin (0.75 units/kg). Blood was collected from the tail vein before (0 min) and at 15, 30, 60, and 120 min after glucose or insulin injection to measure the glucose concentration using a glucometer (Roche, Mannheim, Germany).

Histopathological analysis

Mouse liver samples were fixed in 4% paraformaldehyde, processed for paraffin or OCT media embedding, and sectioned at 5 μm thickness. The paraffin-embedded liver sections were carried out hematoxylin and eosin (H&E) staining for histological analysis. Oil Red O staining was performed on frozen sections to determine hepatic steatosis.

Enzyme-linked immunosorbent assay (ELISA)

The concentrations of IL-1β, TNF-α, TGF-β, and IL-10 in the liver were measured with ELISA kits (MultiSciences, ShangHai, China) according to the manufacturer's instructions.

Biochemical analysis

The levels of total cholesterol (TC), triglyceride (TG), low-density lipoprotein cholesterol (LDL-C), high-density lipoprotein cholesterol (HDL-C) and hepatic TC, TG, were detected by biochemical kits (Nanjing Jiancheng Bioengineering Institute, Nanjing, China) according to the manufacturer's instructions.

Isolation and characterization of Exos

For the transmission electron microscopy (TEM) analysis, the approximately 5 μL of the Exosome (Exos) suspension sample was firstly applied onto a carbon-coated copper grid, adsorbed at RT for 10 min, followed by staining with 2% phosphotungstic acid solution (pH=6.5) at RT for 2 min. After the sample was dried, the morphology of the Exos was observed by HT7700 TEM (Hitachi, Tokyo, Japan). Western blot was used for the identification of Exos membrane markers with the following primary antibodies: CD63 (ab217345, Abcam, MA, USA), CD9 (A19027, ABclonal, Wuhan, China), and TSG101 (ab125011, Abcam). To evaluate the absolute size distribution and concentration of Exos, Exos were analyzed by Flow Nanoanalyzer (NanoFCM Inc., Xiamen, China) according to the manufacturer's instructions.

Cell culture and coculture system

Primary hepatocytes were isolated as previously described[1]. $CD4^+$ $CD25^+$ Treg cells were purified from the mouse spleen with EasySep™ Mouse $CD4^+$ $CD25^+$ Regulatory T Cell Isolation Kits (Stem Cell Technologies, Vancouver, Canada).

For co-culture study, the primary hepatocytes cocultured with (1:1 ratio) or without Tregs, and then stimulated with free fatty acid (FFA) for 72 h, which was prepared at 2:1 ratio (500 μM: 250μM) of oleic acid (OA) to palmitic acid (PA). For the IL-10

neutralizing experiment, 10 μg/ml mouse IL-10 antibody (MAB417, R&D systems, Minneapolis, USA) was added to the coculture system. To assess insulin signaling, the hepatocytes were stimulated with 5 μg/mL insulin for 15 min before collection. For lipid staining, the hepatocytes were subjected to oil red O staining (C0158, Beyotime, Shanghai, China) according to the manufacturer's instructions.

BMDMs were prepared as a previous description[2]. BMDMs were treated with 100 ng/mL LPS and 250 μM PA for 12 h. The same volume of PBS was used as a control treatment. Naïve $CD4^+$ T cells were purified from the mouse spleen using EasySep™ Mouse naïve $CD4^+$ T Cell Isolation Kits (Stem Cell Technologies) (purity> 90%).

For the Treg differentiation assay, naïve $CD4^+$ T cells were cocultured with BMDMs (1:1 ratio). Cells were cultured in RPMI 1640 complete medium containing soluble anti-CD3 (1 μg/ml) (100340, Biolegend), soluble anti-CD28 (1 μg/ml) (102116, Biolegend), and recombinant murine IL-2 (5 μg/ml) (212-12, Peprotech). After 3 days, cells were harvested for Foxp3 analysis.

To verify the role of Exos, BMDMs were pretreated with 5 μM GW4869 (D1692, Sigma-Aldrich, St. Louis, USA) or DMSO for 6 h, then they were cocultured with naïve $CD4^+$ T cells for 3 days, during which GW4869 treatment was continuously performed.

For the coculture of Exos and naïve $CD4^+$ T cells, after BMDMs were stimulated with LPS and PA as described above, the medium was changed, and Exos were collected as described below. Naïve $CD4^+$ T cells were prestimulated with soluble anti-CD3 (1 μg/ml), soluble anti-CD28 (1 μg/ml), and recombinant murine IL-2 (5 ng/ml) for 3 days. The Exos (30 μg/ml) were added to the system, and coculture was continued for 3 days.

Exosome-labelling for cellular uptake

The purified Exos were labeled with PKH26 membrane dye (MINI26, Sigma Aldrich) according to the manufacturer's protocol. PKH26-labeled Exos were added to naïve $CD4^+$ T cells and incubated for 8 h. Then the specific uptake of PKH26-labeled Exos by cells was visualized by the confocal microscopy (Leica Microsystems, Wetzlar, Germany).

Plasmid Constructs and Transfections.

The plasmid pEF-Flag-NICD (Notch1 intracellular domain) was constructed as follows: The NICD fragments were amplified using cDNA obtained from mouse BMDMs and subsequently inserted into the EcoRI and XbaI sites of pEF-Flag-N. The plasmid was then transferred into BMDMs with Lipo8000 transfection reagent (C0533, Beyotime) according to the manufacturer's instructions.

Transfection of miRNA mimic and miRNA inhibitor

The miR-142a-3p mimic with its miRNA negative control (NC), and miR-142a-3p inhibitor with its NC were purchased from RiboBio (Guangzhou, China). Naïve $CD4^+$ T cells were prestimulated with soluble anti-CD3 (1 μg/ml), soluble anti-CD28 (1 μg/ml), and recombinant murine IL-2 (5 ng/ml) for 3 days. After that, naïve $CD4^+$ T cells were transfected with 50 nmol/L miRNA mimic or 100 nmol/L miRNA inhibitor, and their corresponding NC using Lipo8000 transfection reagent.

Western Blot

Cells or Exos were lysed using lysis buffer and quantified by BCA assay. Equal amounts of proteins were separated on a 12% SDS-PAGE and then transferred to a

polyvinylidene difluoride membrane (Millipore, Bedford, MA). The membranes were blocked with 5% skim milk. Afterward, primary antibodies were incubated overnight at 4°C, followed by HPR-conjugated secondary antibodies. Protein bands were visualized using gel imaging analyzer (Peiqing, Shanghai, China). The used primary antibodies included anti-GAPDH (PMK053M, bioprimacy, Wuhan, China), anti-β-actin (PMK083M, bioprimacy), anti-β-tubulin (PMK088M, bioprimacy), anti-Cleaved Notch1 (4147, Cell Signaling Technology), anti-Akt (4691, Cell Signaling Technology), anti-p-Akt (4060T, Cell Signaling Technology), anti-CD9, anti-CD63, anti-TSG101.

Quantitative RT-PCR Analysis

Total RNA was prepared using Trizol extraction. The cDNA was synthesized by miRNA 1st Strand cDNA Synthesis Kit (Vazyme Biotech, Nanjing, China) (for miRNA) or PrimeScript RT Reagent Kit (Takara, Tokyo, Japan) (for mRNA) according to the manufacturer's protocol. The expression of miRNA and mRNA were estimated by a real-time PCR system (Bio-Rad Laboratories, CA, USA) using SYBR qPCR Master Mix (Vazyme Biotech). β-actin or U6 were used as internal controls. Data were then analyzed using the ΔΔCt method. The primer sequences used in this study are listed in Table S1.

Immunofluorescence (IF) staining

For $CD4^+$ T cells, Foxp3 staining was performed with Foxp3 antibody (Zenbio, Chengdu, China). Human liver macrophage cleaved Notch1 intensity was assayed by co-staining sections with anti-CD68 (ab213363, Abcam) and cleaved Notch1 (4147T,

Cell Signaling Technology) antibodies. DAPI was used as nuclear staining. IF images were obtained using Olympus BX50 microscope.

Luciferase reporter assay

The wild-type (WT) and mutated (MT) sequences containing miR-142a-3p binding sites was amplified by PCR and cloned them into pmirGLO vector (Promega, Madison, WI, USA) to reconstructed luciferase reporter plasmids. Then, 100 ng WT or MT vectors were co-transfected with 50nM miR-142a-3p into HEK293T cells at 70% confluence using Lipo8000 transfection reagent. After 48 h, cells were collected and firefly luciferase and renilla activities were detected using Dual-Luciferase Reporter Assay System ((Vazyme Biotech). Data were normalized by calculating the ratio of firefly luciferase activity to Renilla luciferase activity.

Quantification and statistical analysis

Data were presented as the mean ± SD. Differences between the two groups were compared using the Student t-test, and comparisons among multiple groups were analyzed with one-way ANOVA followed by Tukey's post hoc test. All Data were analyzed using Prism 7.0 (GraphPad Software) for statistical significance. Differences were considered significant at P value <0.05.

Supplementary figures

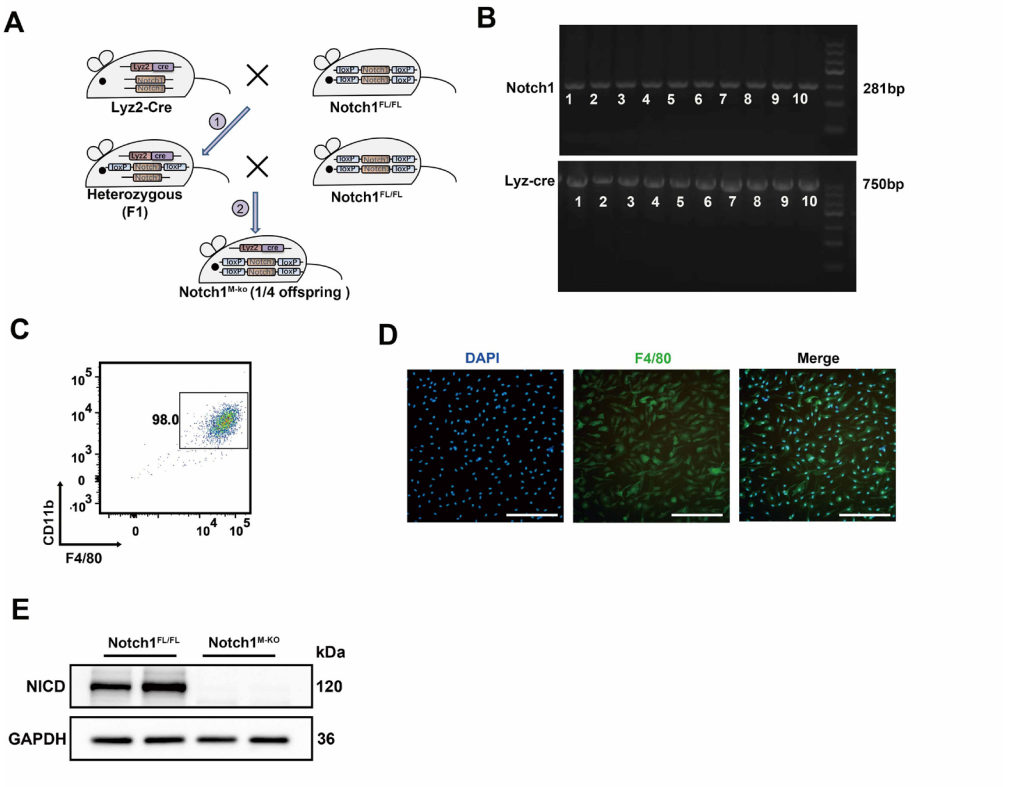

Fig. S1. Generation and characterization of Notch1$^{M\text{-}KO}$ mice. (A) Diagram of the production of Notch1$^{M\text{-}KO}$ mice. (B) PCR identified the genotypes of Notch1$^{M\text{-}KO}$ mice. (C) F4/80^{+}CD11b^{+} BMDMs from mice were detected by flow cytometry. (D) Representative pictures of immunofluorescence staining of F4/80^{+} BMDMs (scale bar: 50 μm). (E) Western blot of BMDMs from Notch1$^{FL/FL}$ and Notch1$^{M\text{-}KO}$ mice. Abbreviations: BMDMs, bone marrow-derived macrophages.

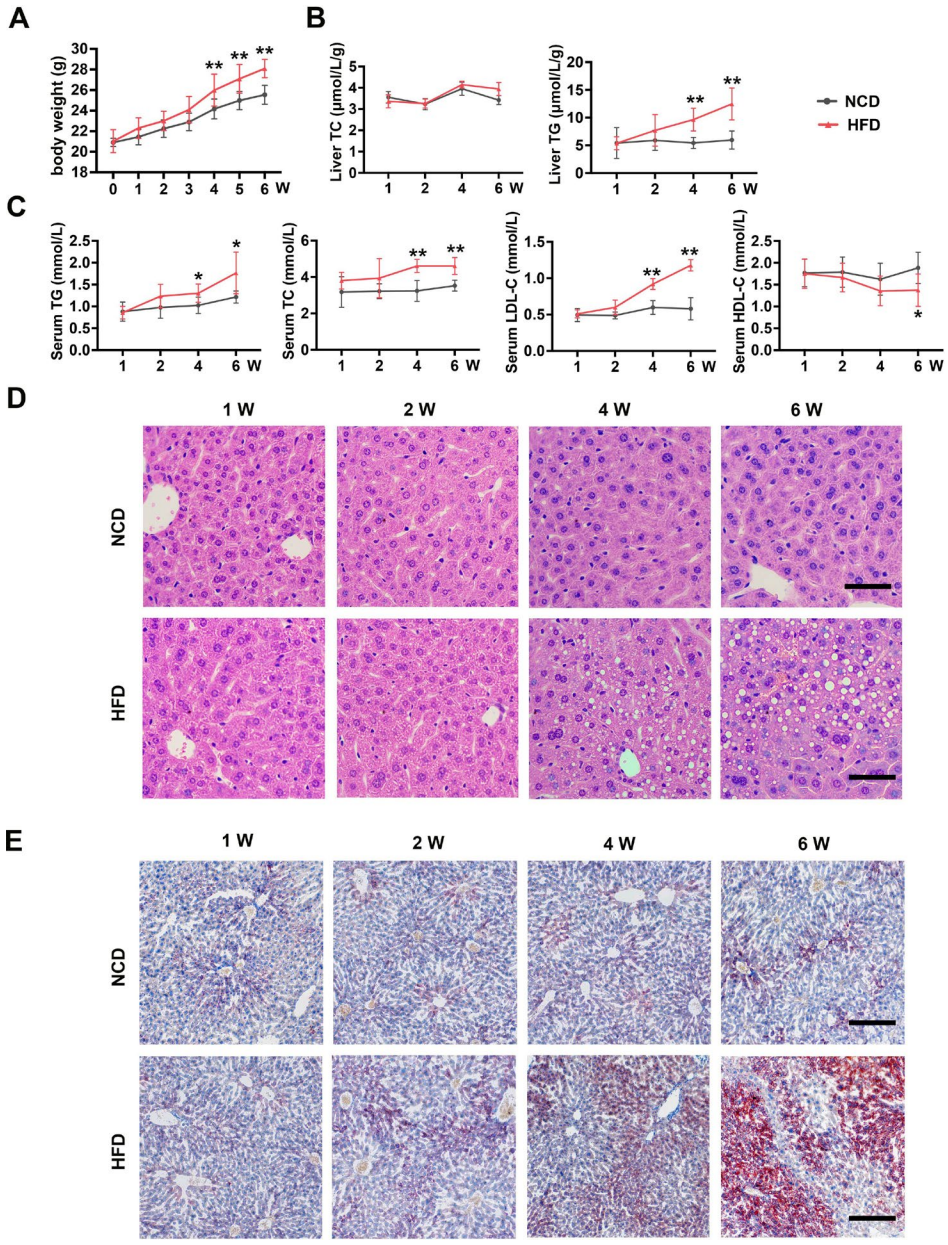

Fig. S2. Wild-type C57BL/6 mice were fed with NCD or HFD for 1, 2, 4, and 6 weeks. Dynamic changes of (A) body weight, (B) liver TG and TC levels, (C) serum TG, TC, LDL-C, HDL-C levels of NCD and HFD mice fed for 1, 2, 4, and 6 weeks (n = 8/group). (D) Representative pictures of H&E staining of liver sections (scale bar: 50 μm). (E) Representative pictures of Oil Red O staining of liver sections (scale bar: 100 μm). Values represent means ± SD. Statistical analysis was performed by two-tailed unpaired Student t-test. **P*< 0.05, ***P* < 0.01. Abbreviations: normal chow diet, NCD; HFD, high-fat diet; TC, total cholesterol; TG, triglyceride; HDL-C, high-density lipoprotein cholesterol; HFD, high-fat diet; LDL-C, low-density lipoprotein cholesterol; H&E, hematoxylin and eosin.

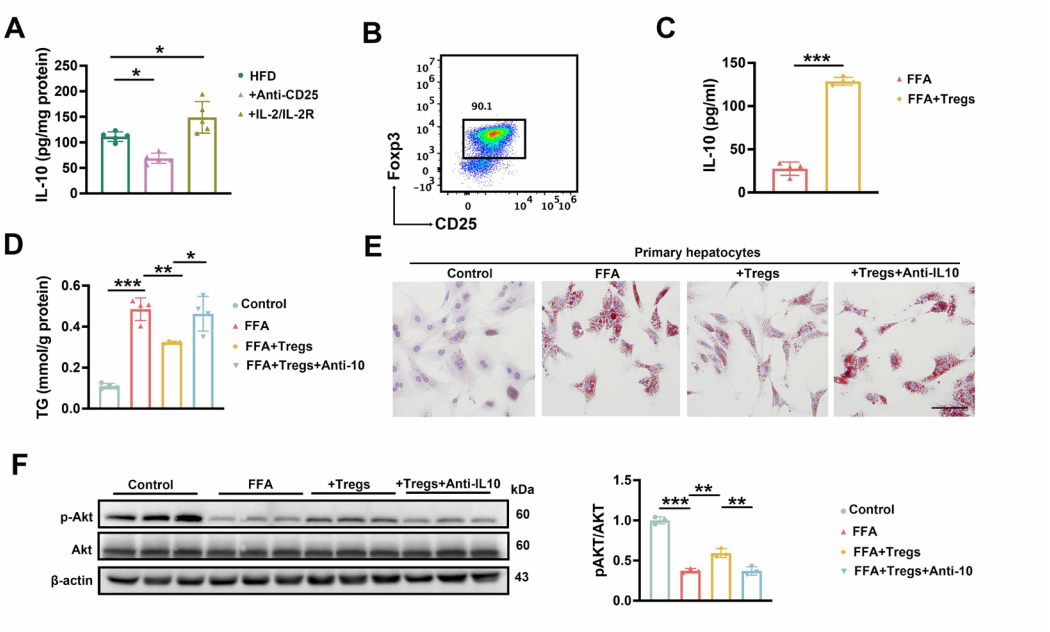

Fig. S3. (A) Wild-type C57BL/6 mice were injected intraperitoneally with anti-CD25 antibody or ldIL-2 once a week to construct Tregs-depletion mice and Tregs-expansion mice, respectively, while fed HFD for 4 weeks. The level of IL-10 in the liver was measured (n=5/group). (B) Tregs isolated from mice spleen were identified by flow cytometry. (C) The amount of IL-10 in the supernatant after primary hepatocytes co-cultured with Tregs or not were treated with FFA for 72 h (n=4/group). (D) TG content (n=4/group), (E) representative pictures of Oil Red O staining (scale bar: 100 μm), (F) immunoblot analysis of insulin-stimulated Akt and p-Akt (n=3/group) of the primary hepatocytes, or cells in cultures with the addition of Tregs and neutralizing antibody IL-10. Values represent means ± SD. Statistical analysis was performed by (A, D, F) one-way ANOVA, Tukeys test or (C) two-tailed unpaired Student t-test. **P*< 0.05, ***P* < 0.01, ****P* < 0.001. Abbreviations: ldIL-2, low-dose IL-2; Treg, regulatory T cell; HFD, high-fat diet; FFA, free fatty acid; IL-10, interleukins-10; TG, triglyceride; pAkt, phosphorylated Akt.

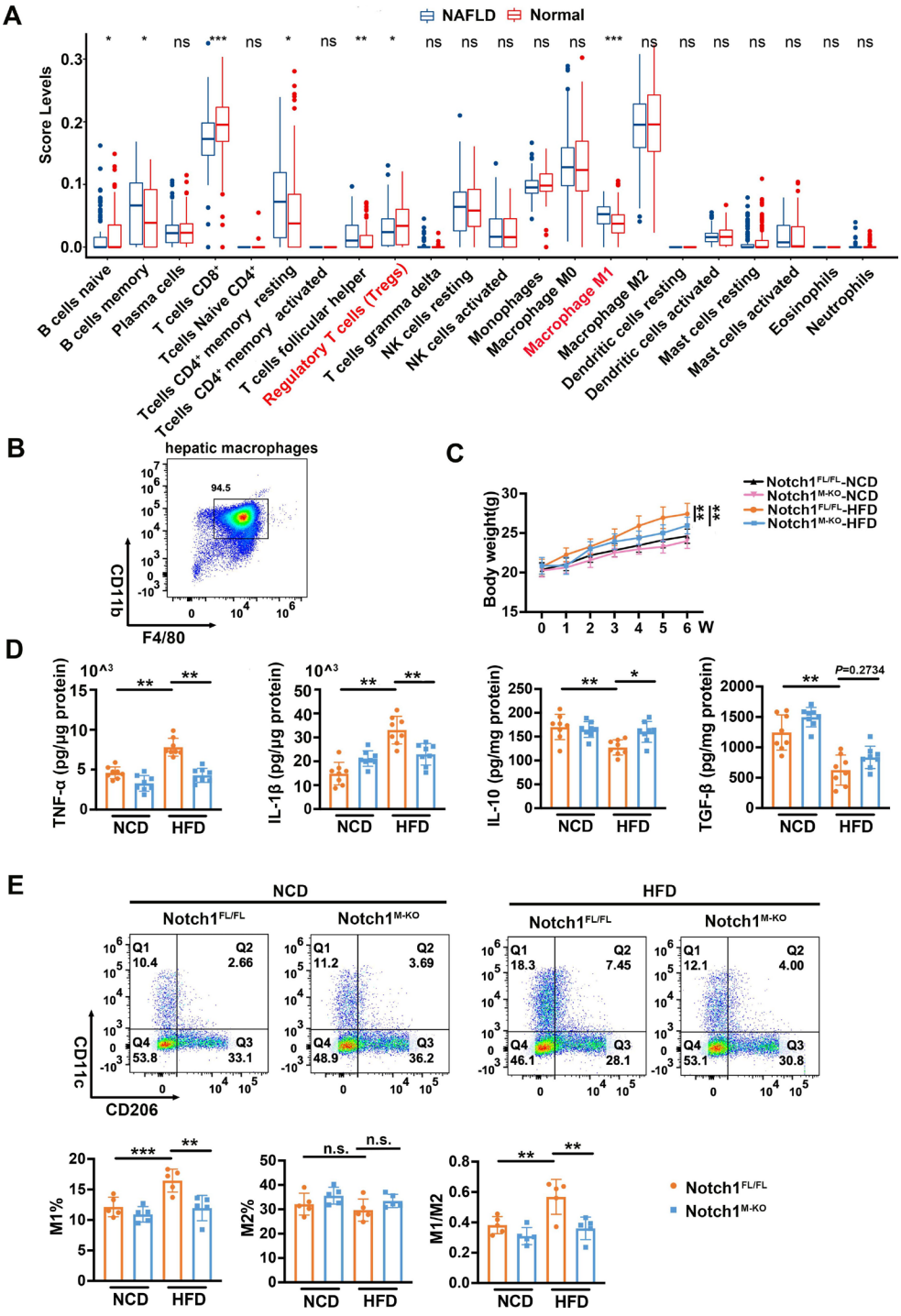

Fig. S4. (A) Bioinformatics analysis of a GEO public dataset (GEO: GSE83452) for frequency of various immune cell types in the liver of NAFLD patients. Notch1$^{FL/FL}$ mice and Notch1$^{M\text{-}KO}$ mice were fed with NCD or HFD for 6 weeks. (B) The purity of the hepatic macrophages separation. (C) The body weight was measured (n=8/group). (D) Levels of TNF-α, IL-1β, IL-10 and TGF-β in the liver (n=8/group). (E) The proportion of M1 (F4/80^{+}CD11c^{+}) and M2 (F4/80^{+}CD206^{+}) macrophages in the liver

(n=5/group). Values represent means ± SD. Statistical analysis was performed by one-way ANOVA, Tukeys test. *P< 0.05, **P < 0.01, ***P < 0.001. Abbreviations: NCD, normal chow diet; HFD, high-fat diet; TNF-α, tumor necrosis factor-α; IL-1β, interleukins-1β; IL-10, interleukins-10; TGF-β, transforming growth factor-β.

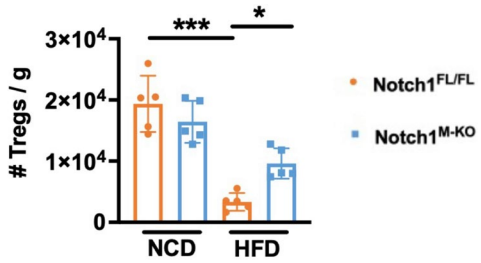

Fig. S5. Notch1$^{M\text{-}KO}$ mice and Notch1$^{FL/FL}$ mice were fed with NCD or HFD for 6 weeks, respectively. The number of Tregs in the livers of Notch1$^{M\text{-}KO}$ mice and Notch1$^{FL/FL}$ mice were analyzed by flow cytometry. Values represent means ± SD. Statistical analysis was performed by one-way ANOVA, Tukeys test. *P< 0.05, ***P < 0.001. Abbreviations: NCD, normal chow diet; HFD, high-fat diet.

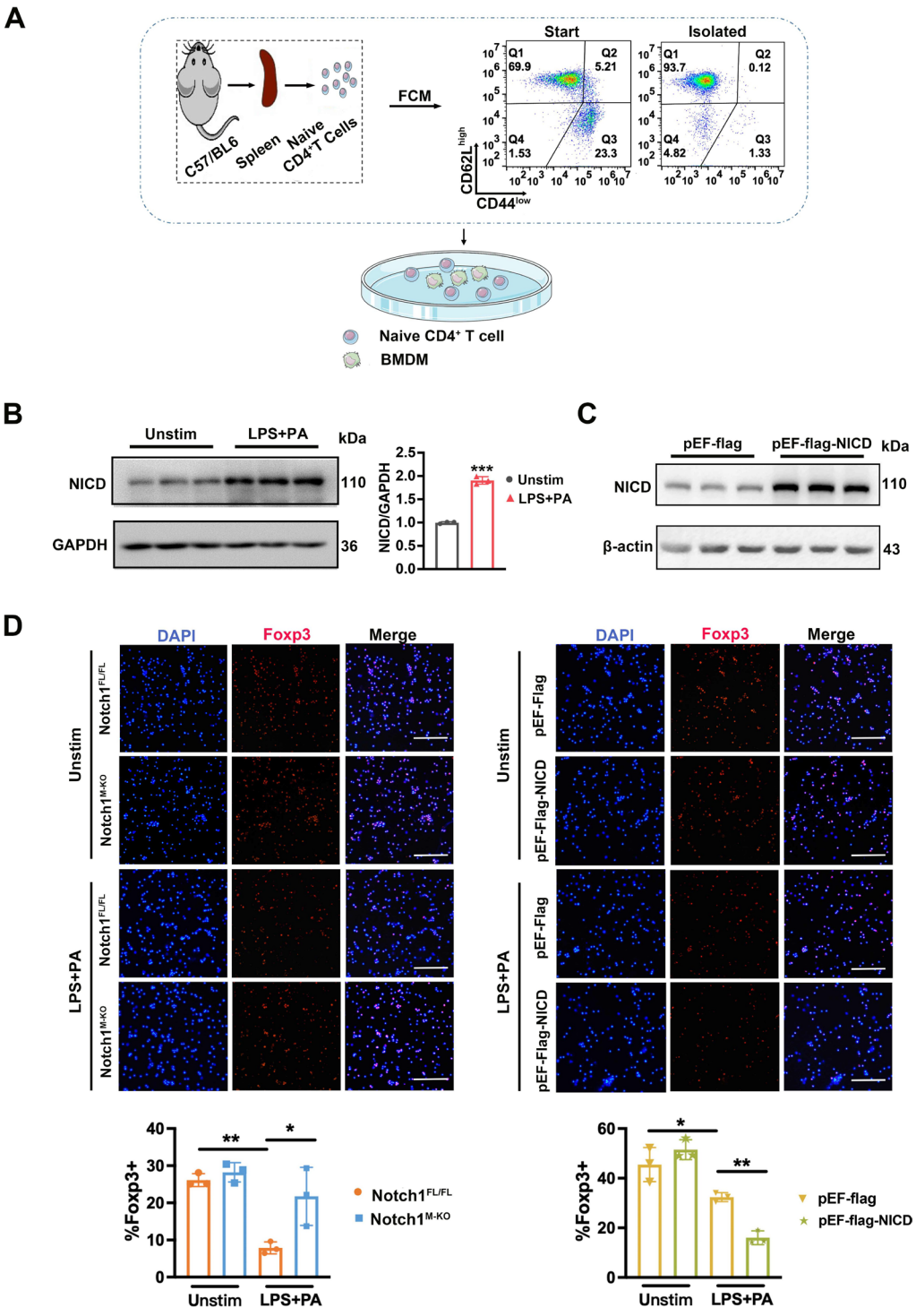

Fig. S6. (A) Schematic of naïve $CD4^+$ T cells isolated from mice spleen with purity! 90% and cocultured with BMDMs. (B) Protein expression of NICD in BMDMs after LPS (100 ng/mL) and PA (250 μM) treatment for 12 h (n=3/group). (C) The overexpression efficiency of NICD was assessed by Western Blot. (D) BMDMs from $Notch1^{FL/FL}$ and $Notch1^{M\text{-}KO}$ mice, the pEF-Flag-NICD or pEF-Flag transfected BMDMs were stimulated with LPS (100 ng/mL) and PA (250 μM) or PBS for 12 h,

respectively, and then co-cultured with naïve CD4$^+$ T cells for 3 days, the representative pictures of IF staining of T cells (scale bar: 200 μm).Values represent means ± SD. Statistical analysis was performed by two-tailed unpaired Student t-test. *P< 0.05, **P < 0.01, ***P < 0.001. Abbreviations: LPS, lipopolysaccharides; PA, palmitic acid; BMDMs, bone marrow-derived macrophages; NICD, Notch1 intracellular domain.

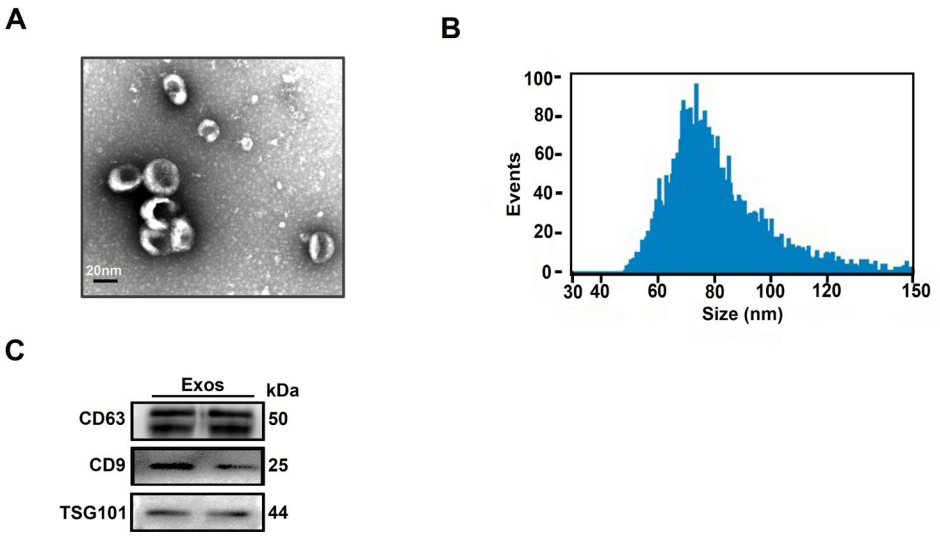

Fig. S7. Identification of Exos isolated from BMDMs. Exos isolated from BMDMs supernatants were analyzed by transmission electron microscopy (A) (scale bar: 20 nm), (B) flow nanoanalyzer, and (C) Western blot. Abbreviations: Exos, exosomes; BMDMs, bone marrow-derived macrophages.

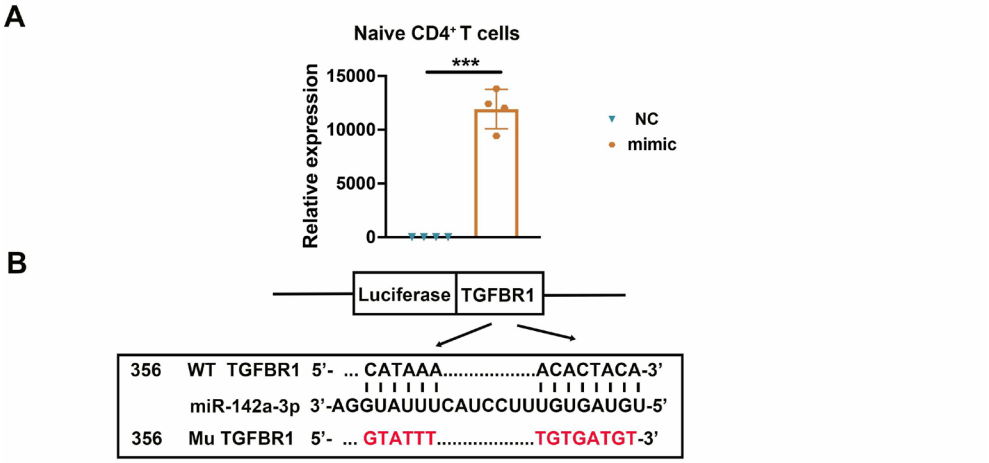

Fig. S8. (A) RT-qPCR analysis of miR-142a-3p in miRNA mimic-transfected naïve CD4$^+$ T cells after 24 h (n=4/group). (B) Schematic of TGFBR1 3'UTR WT and MT luciferase reporter vectors. Values represent means ± SD. ***P < 0.001. Abbreviations: WT, wild-type; MT, mutant; NC, negative control.

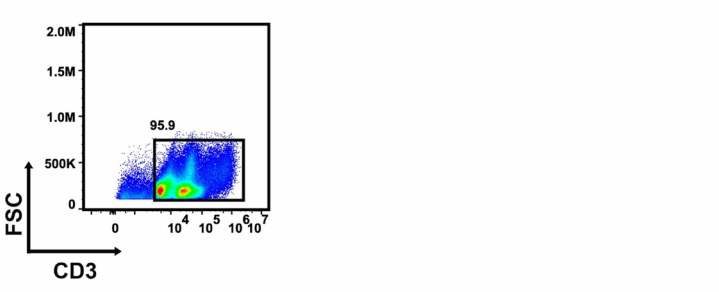

Fig. S.9. The purity assessment of isolated hepatic T cells.

Supplementary tables

Table S1. DNA sequences for mouse genotyping, RT-qPCR.

Genes	Forward (5' to 3')	Reverse (3' to 5')
Lyz2	CCCAGAAATGCCAGATTACG	CTTGGGCTGCCAGAATTTCTCTTACA
	CTTGGGCTGCCAGAATTTCTC	GTCGGCCAGGCTGAC
Notch1	TGCCCTTTCCTTAAAAGTGG	GCCTACTCCGACACCCAATA
Human-β-actin	ATGGGTCAGAAGGATTCCTATGTG	CTTCATGAGGTAGTCAGTCAGGTC
Mouse-β-actin	AGATCATTGCTCCTCCTGAGCGCA	AAACGCAGCTCAGTAACAGTCCGC
Human Foxp3	CAGCACATTCCCAGAGTTCCTC	GCGTGTGAACCAGTGGTAGATC
Mouse Foxp3	CCCAGGAAAGACAGCAACCTT	TTCTCACAACCAGGCCACTTG
U6	CTCGCTTCGGCAGCACA	AACGCTTCACGAATTTGCGT
miR-142a-3p	GCGCGTGTAGTGTTTCCTACTT	AGTGCAGGGTCCGAGGTATT

Table S2. List of antibodies used in this study.

Antibodies	Company	Catalog number	Clone NO.
CD3-FITC	eBioscience	Cat#: 11-0032-82	17A2
CD4-APC	eBioscience	Cat#: 17-0041-82	GK1.5
CD25-PeCy7	eBioscience	Cat#: 25-0251-81	PC61.5
Foxp3-PE	eBioscience	Cat#: 12-4771-82	NRRF-30
F4/80-PeCy7	eBioscience	Cat#: 12-4771-82	BM8
Notch1-PE	Biolegend	Cat#: 12-5785-82	mN1A
IL-10 Antibody	R&D systems	Cat#: AB-417-NA	Polyclonal
CD11c-PE	Biolegend	Cat#: 117308	N418
CD206-APC	Biolegend	Cat#: 141708	MMR
CD4-FITC	eBioscience	Cat#: 11-0041-82	GK1.5
Anti-TGFBR1	Abcam	Cat#: ab31013	Polyclonal
Anti-CD63	Abcam	Cat#: ab217345	EPR21151
Anti-CD9	ABclonal	Cat#: A19027	ARC0330
Anti-TSG101	Abcam	Cat#: ab125011	EPR7130(B)
Anti-CD3	Biolegend	Cat#: 100340	145-2C11
Anti-CD28	Biolegend	Cat#: 102116	37.51
Anti-Notch1	Cell Signaling Technology	Cat#: 4147T	Val1744
Anti-Akt	Cell Signaling Technology	Cat#: 4691T	C67E7
Anti-p-Akt	Cell Signaling Technology	Cat#: 4060T	Ser473
Anti-Foxp3	Zenbio	Cat#: 200501-7H9	7H9
Anti-CD68	Abcam	Cat#: ab213363	EPR20545

References

Author names in bold designate shared co-first authorship

1. **Dong X**, **Feng Y**, Xu D, et al. Targeting macrophagic 17beta-HSD7 by fenretinide for the treatment of nonalcoholic fatty liver disease. *Acta Pharm Sin B*. Jan 2023;13(1):142-156. doi:10.1016/j.apsb.2022.04.003

2. **Yang Y**, **Ni M**, Zong R, et al. Targeting Notch1-YAP Circuit Reprograms Macrophage Polarization and Alleviates Acute Liver Injury in Mice. *Cell Mol Gastroenterol Hepatol*. 2023;15(5):1085-1104. doi:10.1016/j.jcmgh.2023.01.002

Original western blot data

Figure 1

Panel H:

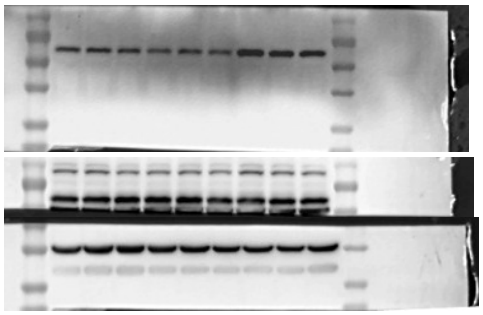

Panel L:

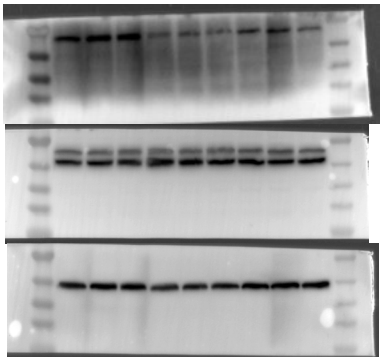

Figure 2

Panel B:

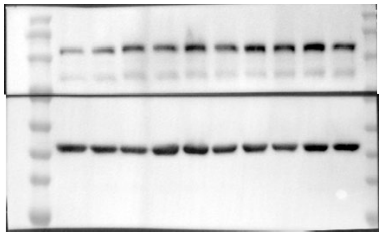

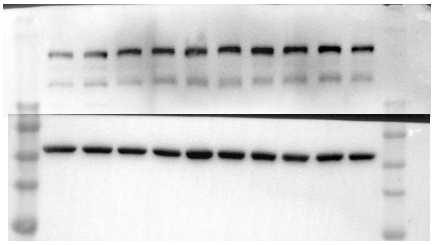

Figure 3

Panel F:

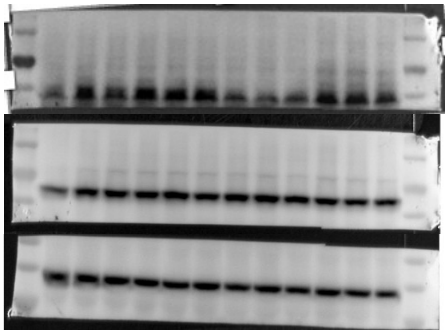

Figure 4
Panel H:

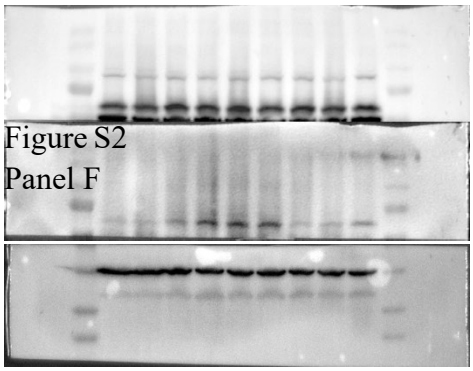

Figure S2
Panel F

Fig. S1
Panel E

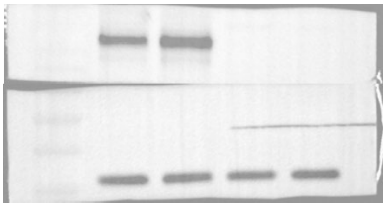

Fig. S3
Panel F

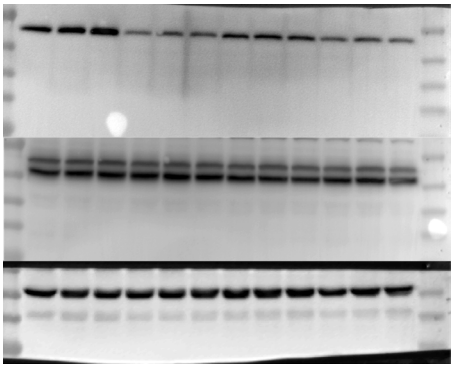

Fig. S6
Panel B

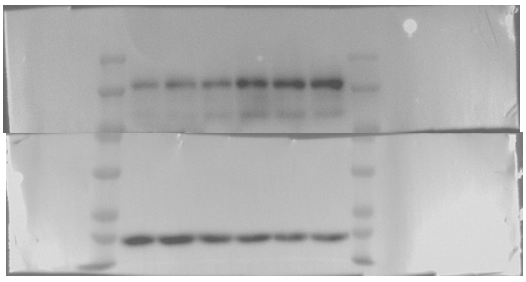

Fig. S6
Panel C

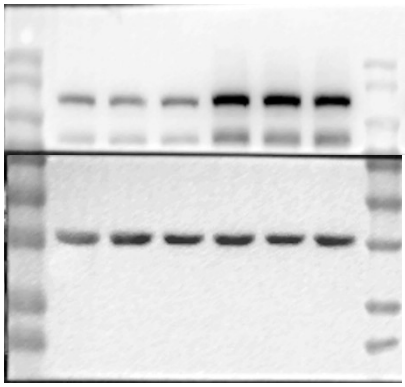

Fig. S7
Panel C
CD63

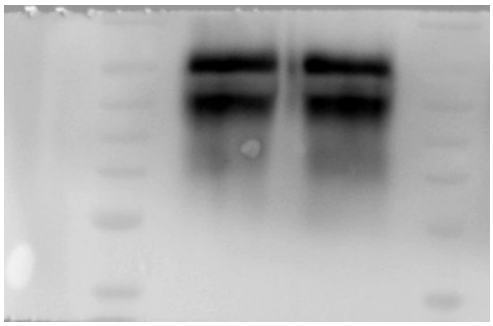

CD9

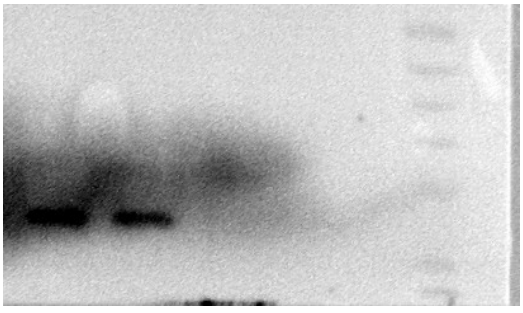

TSG101

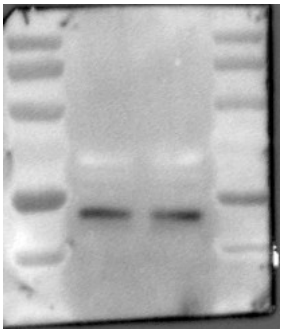

Revision report

TGFBR1

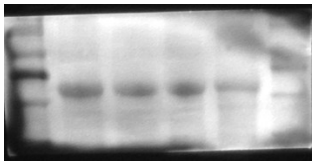

GAPDH